REPUBLIC OF TÜRKİYE
YILDIZ TECHNICAL UNIVERSITY
GRADUATE SCHOOL OF SCIENCE AND ENGINEERING

ANALYSIS OF TOUCHDOWN AND TURBULENCE INTENSITY FOR GENERAL AVIATION AIRCRAFTS USING WAVELET TRANSFORM

Hasan ÖZKAYA

MASTER OF SCIENCE

Department of Control and Automation Engineering

Program of Control and Automation Engineering

Supervisor

Prof. Dr. Ufuk SAKARYA

January, 2025

REPUBLIC OF TÜRKİYE

YILDIZ TECHNICAL UNIVERSITY

GRADUATE SCHOOL OF SCIENCE AND ENGINEERING

ANALYSIS OF TOUCHDOWN AND TURBULENCE INTENSITY FOR GENERAL AVIATION AIRCRAFTS USING WAVELET TRANSFORM

A thesis submitted by Hasan ÖZKAYA in partial fulfillment of the requirements for the degree of **MASTER OF SCIENCE** is approved by the committee on 24.01.2025 in Department of Control and Automation Engineering, Program of Control and Automation Engineering.

Prof. Dr. Ufuk SAKARYA
Yildiz Technical University
Supervisor

Approved By the Examining Committee

Prof. Dr. Ufuk SAKARYA, Supervisor
Yildiz Technical University _____

Assoc. Prof. Dr. Muhammet Ali KARABULUT, Member
National Defence University _____

Assist. Prof. Dr. Mumin Tolga EMİRLER, Member
Yildiz Technical University _____

I hereby declare that I have obtained the required legal permissions during data collection and exploitation procedures, that I have made the in-text citations and cited the references properly, that I haven't falsified and/or fabricated research data and results of the study and that I have abided by the principles of the scientific research and ethics during my Thesis Study under the title of "Analysis of Touchdown and Turbulence Intensity for General Aviation Aircrafts Using Wavelet Transform" supervised by my supervisor, Prof. Dr. Ufuk SAKARYA. In the case of a discovery of false statement, I am to acknowledge any legal consequence.

Hasan ÖZKAYA

Signature

Dedicated to my family

and my love

ACKNOWLEDGEMENTS

I would like to thank everyone who guided me, contributed to me, and supported me throughout the preparation of this thesis.

First of all, I would like to thank my thesis supervisor Prof. Dr. Ufuk SAKARYA for always supporting me, providing me with guidance and patiently guiding me. His important contributions and suggestions during my research process have increased the quality of this study.

In addition, I would like to thank my family and girlfriend who have always been a source of morale, encouraged me, and never withheld their support even for a moment. Your being with me at all times has been my greatest source of strength during this process.

Finally, I would like to express my gratitude to Baykar Technology Company and my valuable managers who encouraged me to attend my classes throughout my graduate education and provided me with the simulation facilities used in the thesis study.

Hasan ÖZKAYA

TABLE OF CONTENTS

LIST OF SYMBOLS

$u_k(t)$	k^{th} Mode in the Time Domain
ρ	Air Density
v	Airspeed
α	Angle of Attack, Angular Acceleration
$\omega_k(t)$	Central Frequency of the k^{th} Mode
γ	Climb Angle of the Aircraft
K_p	Coefficient of the Feedback P Controller
ψ^*	Complex Conjugate Equivalent of the Wavelet Function
$*$	Convolution Operation
a	Dilation Parameter
$\delta(t)$	Dirac Delta Function
q	Dynamic Pressure
E	Energy of the Function
$x(t)$	Examined Continuous Signal in Time Domain
F	Force
$\hat{\psi}(f)$	Fourier Transform of the Wavelet Function
λ	Lagrange Multipliers
C_l	Lift Coefficient
L	Lift Force
b	Location Parameter
m	Mass
$m(t)$	Mean Envelope Function
I	Moment of Inertia
N	Number of Elements
K	Number of Modes
θ	Pitch Angle of the Aircraft
$h(t)$	Proto Intrinsic Mode Function
$r(t)$	Residue Signal

$f_{sampling}$	Sampling Frequency
β	Slip Angle of the Aircraft
$\mathcal{L}$	The Loss Function Used in the Optimization Problem
t	Time
∂_t	Time Derivative
τ	Torque
I_T	Turbulence Intensity
$\psi(t)$	Wavelet Functions
W	Weight
$w(a)$	Weighting Function
A	Wing Area

LIST OF ABBREVIATIONS

ADMM	Alternating Direction Method of Multipliers
CAT	Clear Air Turbulence
CEEMD	Complementary Ensemble EMD
CWT	Continuous Wavelet Transform
DWT	Discrete Wavelet Transform
EASA	European Union Aviation Safety Agency
EEMD	Ensemble EMD
EMD	Empirical Mode Decomposition
FAA	Federal Administration Aviation
GNSS	Global Navigation Satellite System
IAS	Indicated Air Speed
IMF	Intrinsic Mod Function
IMU	Inertial Measurement Unit
MEMD	Multivariate EMD
NA	Noise-Assisted
SEAT	Single Engine Air Tanker
STFT	Short Time Fourier Transform
VMD	Variational Mode Decomposition
WT	Wavelet Transform

LIST OF FIGURES

LIST OF TABLES

ABSTRACT

Analysis of Touchdown and Turbulence Intensity for General Avıatıon Aircrafts Using Wavelet Transform

Hasan ÖZKAYA

Department of Control and Automation Engineering

Program of Control and Automation Engineering

Master of Science Thesis

Supervisor: Prof. Dr. Ufuk SAKARYA

This study aims to increase the flight safety of general aviation aircraft, which are technologically behind other aircraft due to their generally low-budget production. By determining the flight stages where aircraft encounter the most accidents and crashes, virtual sensors that will increase the situational awareness of pilots and autopilot systems were created in these stages. One of the situations detected with the virtual sensor is the detection of the aircraft's touchdown with the ground and the other is the detection of the turbulence level in the environment. In the detections made, the data collected from the IMU sensors integrated into the aircraft were processed with three different methods and the methods were compared with each other. The methods used can be listed as Continuous Wavelet Transform, Empirical Mode Decomposition and Variational Mode Decomposition. According to the experimental studies, it has been shown that the proposed detection methods largely eliminate the unwanted frequency effects compared to the compared methods and give promising results.

Keywords: Touchdown, turbulance, aviation, aircraft, virtual sensing, wavelet, CWT, EMD, VMD

ÖZET

Dalgacık Dönüşümü Kullanılarak Genel Havacılık Uçakları İçin İniş ve Türbülans Yoğunluğunun Analizi

Hasan ÖZKAYA

Kontrol ve Otomasyon Mühendisliği Anabilim Dalı
Kontrol ve Otomasyon Mühendisliği Programı
Yüksek Lisans Tezi

Danışman: Prof. Dr. Ufuk SAKARYA

Bu çalışmada, genellikle düşük bütçeli üretimlerinden dolayı teknolojik olarak diğer hava araçlarından geride kalan genel havacılık uçaklarının uçuş güvenliklerinin artırılması amaçlanmaktadır. Hava araçlarının en çok kaza ve kırım ile karşılaştıkları uçuş aşamaları tespit edilerek bu aşamalarda pilotların ve otopilot sistemlerinin durumsal farkındalıklarını artıracak sanal algılayıcılar oluşturulmuştur. Sanal algılayıcı ile tespiti yapılan durumlardan biri uçağın yere temasının tespiti ve diğeri bulunduğu ortamdaki türbülans seviyesinin tespitidir. Yapılan tespitlerde, uçağa entegre edilen IMU sensörlerinden toplanan veriler üç farklı yöntem ile işlenmiş ve yöntemler birbirleri ile karşılaştırılmıştır. Kullanılan yöntemler sürekli dalgacık dönüşümü, ampirik kip ayrışımı, ve varyasyonel kip ayrışımı olarak listelenebilir. Yapılan deneysel çalışmalara göre, önerilen tespit yöntemlerinin karşılaştırılan yöntemlere göre istenmeyen frekans etkilerini büyük ölçüde temizlediği ve umut verici sonuçlar sunduğu gösterilmiştir.

Anahtar Kelimeler: Yere temas, türbülans, havacılık, uçak, sanal algılama, kabarcık, CWT, EMD, VMD

1
INTRODUCTION

Humanity has acquired new abilites by observing nature and its environment throughout history. Regarding the ancient paintings on the cave walls and figures on simple tools found in archaeological studies, birds are among the things that have been observed from the very beginning. Since birds can be used in different ways such as making food, clothing and simple tools, they are likely to be among the creatures that are frequently focused and observed people's daily life. Undoubtedly, this observation is what initiated the desire to fly in human beings. In fact, even the word "aviation," which is frequently used today, is derived from the Latin root "awi" which means bird [1].

When looking at the written and oral sources that transferred from past to present, it is possible to see refleciton of the desire to fly in many cultures, religious and mythological elements. The story of Icarus of Athens from Greek mythology and Hezarfen Ahmet Çelebi's flight to the Galata Tower in Evliya Çelebi's narratives are popular examples that occurs when considering humanitiy's desire to fly. After such physical flight experiments, which can be considered the most primitive form of aviation, it is seen that in the 18th century, flight experiments with lighter-than-air vehicles such as hot air balloons began. Subsequently in the 20th century, the first recorded controlled flight with a heavier-than-air vehicle was made by the Wright brother. Following this flight, in virtue of the studies carried out on aviation and aircraft technology throughout the 20th century, great developments have taken place and modern aviation has been brought to where it is today [2].

Considering the progress made since the Wright brothers' first prototype, fixed-wing aircraft today have numerous different purposes and areas of use. Aircrafts have been game-changing tools in different fields, from agriculture to intelligence, from meteorology to aerobatics and to battlefields. Since they have such a wide

usage area, it is possible to come across airpcrafts of different sizes and features specialized according to their usage areas.

When evaluated in terms of hardware sophistication, fifth-generation fighter aircraft currently in military service and sixth-generation fighter aircraft, whose initial prototypes are under development, can be identified as having the most advanced technological equipment. On the other hand, aircrafts with the lowest level of equipment are low-cost civil aviation aircrafts used for hobby and training purposes. General purpose civil aviation aircraft lag behind their commercial and military equivalents with respect to both security systems and electronic/sensory hardware capabilities.

In this study, two different situations that endanger the safety of all aircrafts, including general purpose civil aircrafts, commercial aircrafts, and military aircrafts, will be discussed. One of the situations is the detection of the aircraft's touchdown and the other is the detection of turbulence. These detection operations will be carried out with the virtual sensing method thus system costs and structural complexity will be reduced. Virtual sensing is a method of predicting physical quantities or parameters that are expensive or difficult to measure [3]. As a result of the studies carried out, it is aimed to make these situations that every aircraft is likely to encounter without endangering flight safety, with low cost and a small amount of equipments.

There are three main headings in the next part of the study. In the second heading, the signal processing methods used during the studies are mentioned. In the third heading, ground contact detection is handled by taking a Cessna-172SP model aircraft as a model and using the aircraft's acceleration and angular velocity data. This determination is shown on a theoretical level and the outputs are discussed. In the fourth heading, the effects of turbulent weather conditions on aircraft, especially in terms of firefighting aircrafts (airtankers), are examined and the severity of turbulence is determined. After the effect of turbulence on the aircraft, the action to be taken regarding the air speed of the aircraft in order to reduce the effect is mentioned and the outputs of the study are shown. In the fifth and last heading, the results obtained from the studies are interpreted and future studies and suggestions are discussed.

2
BACKGROUND AND METHODS

In this section, the signal processing methods used in the studies will be explained and fundamental knowledge about the methods will be given. The methods to be explained are as follows:

- Continuous Wavelet Transform
- Empirical Mode Decomposition
- Variational Mode Decomposition

2.1 Continuous Wavelet Transform (CWT)

CWT is a signal processing tool used to perform time-frequency analysis of signals containing time-dependent frequency changes. CWT has many different usage areas such as noise decomposition in signals [4], image compression [5], biomedical signal analysis [6], machine learning [7], audio and image processing [8], structural health monitoring [9] and finance [10].

In this section, the concept of wavelet and the historical development process of CWT will be mentioned, the concept of wavelet will be defined and wavelet transform will be shown. Additionally, some advantages of wavlet transform over Fourier transform will be highlighted.

2.1.1 History of Wavelet and Wavelet Transform

The term Wavelet, which is thought to have emerged as an imitation of the French word "ondelette", means "small wave" [11]. The term wavelet was first used in the last quarter of the 20th century by French geophysicists Jean Morlet and Alex Grossmann. Morlet and Grossmann named the functions they used in their studies on the analysis of seismic waves as Wavelet. In addition to this naming, they also announced the formulation of the wavelet transform, which is now called

Continuous Wavelet Transform (CWT), with a publication in 1984 [12]. Afterward, in the late 1980s and early 1990s, Ingrid Daubechies developed the wavelet transform theory by introducing orthonormal wavelet bases that enable the use of Discrete Wavelet Transform with her studies [13]. With these developments, the theory and practice of wavelet transform have been linked since the 1990s, and many academic studies based on wavelet transform have been published. Today, wavelet transform is used for different purposes in many different sectors.

2.1.2 The Wavelet

Wavelets are wave-shaped and oscillating signals that contain both frequency and time components. Wavelets serve as a template for the signal to be processed when used with a signal processing tool called wavelet transform. There are many different wavelets that can be used depending on the nature of the signal to be processed and the result desired to be obtained. Figure 2.1 shows the time representation of some of the popular wavelets that are frequently used.

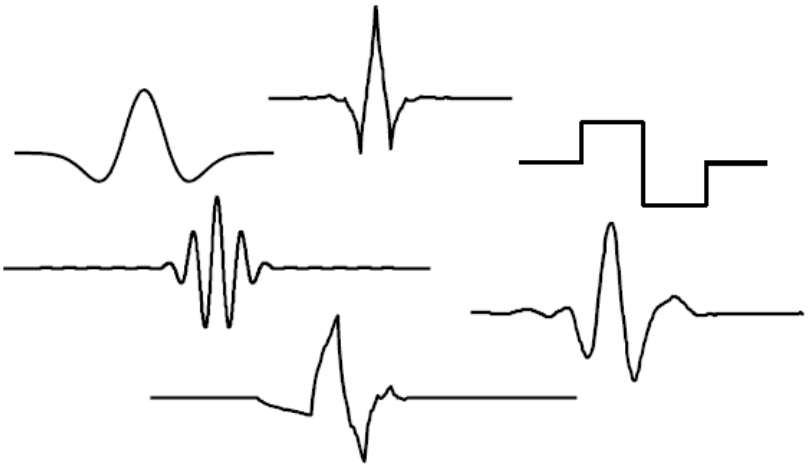

Figure 2.1 Some popular wavelet types

Wavelet functions are denoted as $\psi(t)$. As an example, a simplified formulation of Mexican Hat Wavelet is given in Equation (2.1).

$$\psi(t) = (1 - t^2) \cdot e^{-t^2/2} \tag{2.1}$$

In order for a function to be called a wavelet, it must meet three basic requirements. These requirements are as follows [14]:

- The function must be finite: The function to be defined as a wavelet must be finite. This means that when it reaches the steady state, the integral of the function must be a finite number and must have stopped changing.

  This situation is shown by Equation (2.2). Here, E denotes the energy of the function. The function was first processed with the modulus operator, and then the integral was performed by squaring the result.

$$E = \int_{-\infty}^{\infty} |\psi(t)|^2 dt < \infty \tag{2.2}$$

- The function must have zero mean: If representation $\hat{\psi}(f)$ considered as the Fourier transform of the representaiton $\psi(t)$, in this case, for the $\psi(t)$ function to be considered a wavelet, its mean must be zero. This condition can also be expressed by the requirement that the function not have a zero-frequency component. $[\hat{\psi}(0) = 0]$
- If it is a complex function, the Fourier transform must be zero: If the function $\psi(t)$ is a complex function, the Fourier transform of the function must be zero for both real frequencies and imaginary frequencies.

2.1.3 Wavelet Transform

Wavelet transform is the process of converting a certain signal into a new form that is thought to be more useful by using special functions defined as wavelets.

Wavelet transform was found as a result of studies carried out to overcome some limitations in Fourier transform [12]. In its most fundamental form, Fourier transform is the process of decomposing an existing signal into sinus waves of different frequencies. Accordingly, its basic function is to find the frequency components in the signal to be examined. The sinus wave used for analysis has infinite energy. Therefore, high frequency resolution is achieved in a signal examined by Fourier transform [15].

Fourier transform is a highly effective method in the analysis of stationary signals (i.e. signals that do not change in frequency over time), which is already in many uses. However, if there are time-dependent frequency changes in the signal to be examined (that is, if the signal is non-stationary), it may not always be the best alternative. Assume that a non-stationary signal will be examined. If what is desired

to be achieved with this analysis is the knowledge of the frequency components contained in the signal, Fourier transform is a suitable tool. However, when the thing to be examined changes depending on which frequency component is present at what time, Fourier transform becomes insufficient to give results.

One of the popular methods used before the introduction of the wavelet transform for time-frequency analysis of non-stationary signals was "Short Time Fourier Transform" (STFT). STFT is the process of taking the Fourier transform of the examined signal within a certain window function. The determined window function (for example, this function can be a Gaussian function) is considered to cover a finite time interval. STFT fundamentally consists of multiplying this function with the signal to be examined. This method can provide appropriate results for time-frequency analysis when applied at certain time intervals where the signal to be examined can be considered stationary. In other words, drawing an analogy from systems theory, the non-stationary signal is essentially linearized to achieve stationarity before transformation operations are applied.

When the purpose in question is time-frequency analysis, the most obvious disadvantage of STFT is the resolution problem. While low-frequency signal components can be processed in larger time windows, shorter time windows may be sufficient for high-frequency signal components. The window function selected in STFT gives a fixed window length. The effect of window length on time-frequency analysis is as follows:

- Narrow Window → Good Time Resolution + Poor Frequency Resolution
- Wide Window → Good Frequency Resolution + Poor Time Resolution

The advantage of the Wavelet transform (WT) starts at this point. WT provides variable window size for time-frequency analyses. When examining WT fundamentally, WT is the process of determining the similarity relationship between the signal and the wavelet by scaling and shifting a selected wavelet within the signal. Where the similarity is high, the size of the output obtained as a result of the transformation is high, while where the similarity is low, the output size is small.

For WT, an appropriate wavelet is first selected based on the signal to be examined. The selected wavelet function can be compared to the sine function in Fourier transform. This first wavelet function to be used as a template is called "Mother

Wavelet". Then, a wavelet family is created by scaling and shifting the mother wavelet. Each wavelet created by scaling and shifting operations is called "Daughter Wavelet". If $\psi(t)$ is a mother wavelet, each of the daughter wavelet's can be calculated as given by Equation (2.3).

$$\psi\left(\frac{t-b}{a}\right) = \left(1 - \frac{t-b}{a}^2\right) \cdot e^{-\frac{1}{2}\cdot\left[\frac{t-b}{a}\right]^2} \tag{2.3}$$

Here, the parameter that enables the selected wavelet to be shifted on the time axis is the b parameter. b is called "location parameter." The parameter that allows the selected wavelet to be scaled is the a parameter. a is called "dilation parameter." Daughter wavelets are created with different combinations of a and b parameters.

If it is assumed that the examined continuous signal is $x(t)$ and the selected wavelet is $\psi(t)$, it can be formulated as given by Wavelet Transform Equation (2.4).

$$T(a,b) = w(a)\int_{-\infty}^{\infty} x(t)\cdot\psi^*\left(\frac{t-b}{a}\right)dt \tag{2.4}$$

Here, ψ^* represents the complex conjugate equivalent of the selected wavelet function. $w(a)$ is called "weighting function." The weighting function can be chosen depending on the application, but its general use is $\frac{1}{\sqrt{a}}$ for the purpose of ensuring that each wavelet has the same energy. When looking at the expression given in Equation (2.4), one can say that WT is essentially the cross-correlation between the signal under analysis and the set of daughter wavelets [14].

The wavelet transform type mentioned up to this point is called Continuous Wavelet Transform (CWT). "Discrete Wavelet Transform" (DWT), another form of wavelet transform, is obtained by applying the transformation process only at certain points instead of applying it over the entire time space. Using DWT may provide an advantage by reducing the processing capacity in digital systems. In addition, the selected wavelet functions must also be suitable for DWT.

2.2 Empirical Mode Decomposition

EMD is a signal processing tool developed for decomposing and analyzing non-linear and non-stationary signals into their components called Intrinsic Mode

Functions (IMF). It was first introduced by Norden Huang and his colleagues at NASA in 1998. EMD has many different usage areas such as biomedical signal analysis, analaysis of financial data [16], vibration analysis (fault diagnosis for mechanical systems) [17], climate data analysis [18].

In this section, the historical development process of EMD will be mentioned, the differences between EMD and CWT will be mentioned, the concept of IMF will be defined and the signal processing process will be shown. Additionally, various variants of EMD will be highlighted.

2.2.1 History of Empirical Mode Decompositon

Towards the end of the 1990s, it was concluded that the existing methods used for the analysis of non-stationary and non-linear signals were inadequate. Although wavelet analysis and Fourier Transform were found to be effective for stationary and linear signals, they could not fully respond to the complex structure seen in non-stationary and non-linear signals because they could not provide time information. Even though CWT partially eliminated the mentioned deficiencies shown as Table 2.1, it remained limited and incomplete because it was insufficient to explain nonlinear signals and was not an adaptive method like EMD due to its dependence on choices in predefined wavelet functions [19].

Considering these shortcomings, Huang and colleagues developed the EMD method in 1998, in which signals are decomposed according to their local properties. With this method, each of the IMFs (subcomponents of the signals) has a narrow frequency band and gives results by analyzing the time-frequency information of the signal simultaneously [18].

Since EMD works based on the signal's own features and is completely adaptive, it has become a method used in the analysis of non-stationary and non-linear signals [16].

Table 2.1 Comparison of EMD and CWT features

Feature	EMD	CWT
Adaptability	It is adaptive; It discriminates according to signal properties.	It is based on predefined wavelet functions; it is not adaptive.
Base Selection	No basis function required.	The choice of base function affects the results.
Non-linearity	It analyzes non-linear signals well.	It is more suitable for linear signals.
Noise Sensivity	It is sensitive to noise; mode interference may occur.	It is more resistant to noise.
Computational Complexity	It requires less calculations, but iterative operations can take time.	It has higher computational complexity.

2.2.2 Intrinsic Mode Function (IMF)

EMD is a method that uses an iterative process to decompose complex signals into their basic subcomponents called IMFs. They are signal components of IMFs that must meet the following two conditions:

- The number of extrema and zero crossings must either be equal or differ at most by one.
- The mean value of the envelope defined by local maxima and local minima must be zero [18].

2.2.3 The Sifting Process (EMD Algoritgm)

The task of EMD is to separate a signal into independent frequency components so that it can be analyzed more easily. The flow chart of the sifting process of EMD algorithm is given in Figure 2.2.

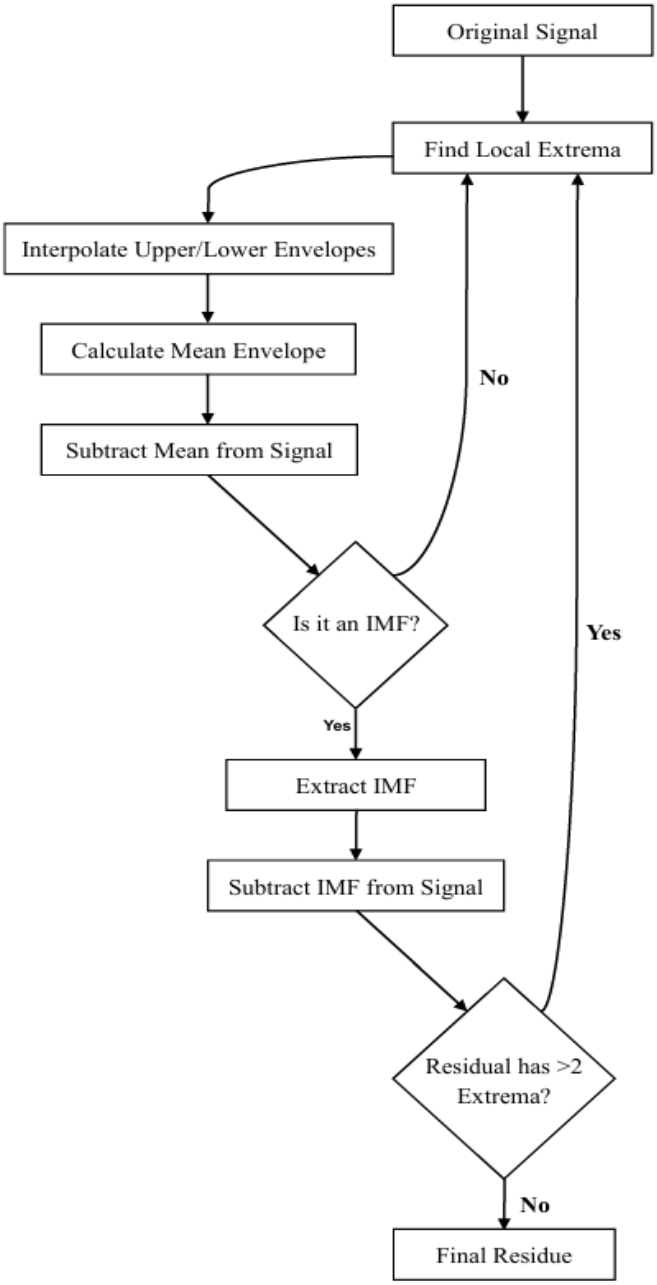

Figure 2.2 The sifting process of EMD algorithm

The relation for decomposing a signal with EMD is given by Equation (2.5).

$$x(t) = \sum_{i=1}^{N} IMF_i(t) + r(t) \tag{2.5}$$

Here $x(t)$ is the original signal, $IMF_i(t)$ is the i[th] intrinsic mode function, $r(t)$ is the residue signal and n is the number of IMF's.

The process of decomposing a signal x(t) with EMD is created by the following steps:

1. All local maximum and minimum points of the signal $x(t)$ are determined.
2. The upper envelope is formed by combining the maximum points, and the lower envelope is formed by combining the minimum points.
3. The mean envelope of the signal is obtained by averaging the upper and lower envelopes. The formula of this calculation is given by Equation (2.6).

$$m(t) = \frac{e_{max}(t) + e_{min}(t)}{2} \tag{2.6}$$

Here $m(t)$ is the mean envelope, $e_{max}(t)$ is the upper envelope and $e_{min}(t)$ is the lower envelope.

4. The mean envelope is substracted from the signal and this process is repeated until the IMF is obtained. The calculation for this process, called Proto-IMF Extraction, is given by Equation (2.7).

$$\textit{Proto-IMF Extraction: } h(t) = x(t) - m(t) \tag{2.7}$$

5. Check is $h\ (t)$ an IMF? Also check two conditions:
    - The number of extrema and zero-crossings must be equal or differ at most by one,
    - The mean value of the envelope must be approximately zero.
6. If $h\ (t)$ is not an IMF:
    - Update $x(t) = h(t)$,
    - Return to the first step.

7. If h(t) is an IMF:
    - Save this IMF,
    - Subtract the IMF from the original signal,
    - Return to first step with the remaining signal.

These processes continue until the signal becomes monotonic, as shown in the Figure 2.2. In the literature, these steps are called "IMF Extraction Criteria" [18] and "Sifting Process Iteration Conditions" [20]. When the signal becomes monotonic (stop condition), it is called "Decomposition Termination Criterion" [21].

The fact that EMD does not need a predefined basis distinguishes it from other time-frequency methods, and the fact that its basis comes from the local characteristics of the signal in an adaptive way makes this method advantageous [18].

2.2.4 Varieties of Empirical Mode Decompositon

EMD has played an important role in the analysis of nonlinear and nonstationary signals. However, due to limitations such as mode interference and sensitivity to noise, new methods and variants have been developed. EMD and its most common variaties is shown by Table 2.2, continue to be used as effective methods in various fields.

Table 2.2 Variants of EMD's, and their puposes and advantages

Variants	Purpose	Advantage
EEMD	Reducing mode interference.	It is noise resistant.
CEEMD	Eliminating residual noise.	Provides higher accuracy.
MEMD	The ability to analyze multivariate signals.	Offers real-time analysis.
NA-MEMD	Noise assisted version of MEMD	Reduces mode mixing problem.

Since the introduction of EMD, several variants have been developed:

- Ensemble EMD (EEMD): It was proposed by Wu and Hang in 2009 to reduce noise sensitivity. White noise was added to each IMF to prevent mode mixing. In this way, more than one EMD was separated and the results were averaged [16].
- Multivariate EMD (MEMD): It was proposed by Rehman and Mandic in 2010. It is made suitable for the analysis of multivariate signals. It enabled multiple input channels to be managed simultaneously and thus maintained relationships between channels [22].
- Noise-Assisted Multivariate EMD (NA-MEMD): It is an improved EMD variant that adds noise channels to the MEMD method to solve the mode mixing problem in multivariate signals. This method gives more effective results, especially in separating low-frequency components and better preserves the frequency relationships between multi-channel signals [23].
- Complementary EEMD (CEEMD): It was proposed in 2011 by Torres et al. It was developed to prevent noise interference. Adds paired (positive and negative) noise to reduce reconstruction error [24].

Empirical Mode Decomposition (EMD) has inspired numerous variants, each designed to address specific limitations or enhance its performance. These adaptations aim to improve decomposition accuracy, noise resistance, and computational efficiency, ensuring EMD remains a versatile tool in signal processing.

2.3 Variational Mode Decomposition (VMD)

VMD was introduced by Dragomiretskiy and Zosso in 2014 as an alternative method to EMD. VMD is a signal decomposition method in which the signal is decomposed into different modes with specific bandwidths. VMD has many different usage areas such as signal noise reduction [25], diagnosis of faults [26], analysis of electrocardiography (ECG) signals [27], structural health monitoring (separation of signals in the analysis of bridges, buildings and structural vibration data and detection of anomalies, if any) [28] and analysis of financial data [29].

In this section, the historical development process of VMD will be mentioned, the differences between VMD and EMD will be mentioned, the methodology of VMD will be explained and the signal processing process will be shown. Additionally, various variants of VMD will be highlighted.

History of Variational Mode Decompositon

VMD was announced by Dragomiretskiy and Zosso in the article published in the IEEE Transactions on Signal Processing journal. The main goal in the development of VMD was to eliminate the disadvantages of EMD such as mode mixing and noise sensitivity as shown by Figure 2.3 [30].

VMD was developed as an alternative to other decomposition methods such as EMD but is a more stable and mathematically formulated method. Comparison of VMD and EMD according to some basic features is given in Table 2.3.

Table 2.3 Comparison of VMD and EMD features

Features	VMD	EMD
Mathematical Foundation	It has a clear mathematical framework based on convex optimization.	EMD also has a mathematical basis, but it is not a fully analytical optimization method.
Mode Interference	There are fewer mode interference problems.	Mode interference occurs frequently.
Noise Sensitivity	It is more resistant to noise.	It is sensitive to noise.
Application Method	Central frequencies are optimized iteratively.	IMFs are extracted by the iterative sifting method.
Speed and Stability	It provides fast and stable parsing.	Decomposition is often slow and unstable.
Customization	The number of modes and bandwidths can ve determined at the beginning.	The number of modes and their features are determined automatically.

2.3.1 Methodology of Variational Mode Decompositon

VMD is the representation of a component concentrated around a central frequency (ω_k) during the decomposition of the signal into band-limited modes. It works by optimizing the modes and keeping the total bandwidth in the signal within the minimum limit range.

Objective Function

The purpose of the VMD is to decompose the $f(t)$ signal, into a certain number of K, modes $u_k(t)$. And the objective function related to this process is given by Equation (2.8):

$$\min_{\{u_k\},\{\omega_k\}} \left\{ \sum_{k=1}^{K} \left\| \partial_t \left[\left(\delta(t) + \frac{j}{\pi t} \right) * u_k(t) \right] e^{-j\omega_k t} \right\|_2^2 \right\} \tag{2.8}$$

Here $u_k(t)$ is the representation of the k^{th} mode in the time domain, $\omega_k(t)$ is the central frequency of the k^{th} mode, * is the convolution operation, $\delta(t)$ is the dirac delta function, j is the complex unit ($j^2 = -1$) and $\|\cdot\|_2^2$ is the L2 norm, which is used to compute the energy of a signal.

The given objective function focuses on the central frequency of each mode and ensures that the total bandwidth is minimized.

Limitation

The limitation of the VMD process is given by Equation (2.9), which states that the signal $f(t)$ should be equal to the sum of all the modes.

$$f(t) = \sum_{k=1}^{K} u_k(t) \tag{2.9}$$

Optimization with Lagrangian Multipliers

$$\mathcal{L} = \alpha \sum_{k=1}^{K} \left\| \partial_t \left[\left(\delta(t) + \frac{j}{\pi t} \right) * u_k(t) \right] e^{-j\omega_k t} \right\|_2^2 + \left\| f(t) - \sum_{k=1}^{K} u_k(t) \right\|_2^2 \tag{2.10}$$

Here $\mathcal{L}$ is the loss function used in the optimization problem, $u_k(t)$ is the k^{th} mode, $\omega_k(t)$ is central frequencies of modes, λ is Lagrange multipliers used in solving optimization constraints, a is the coefficient that controls the weight of the penalty term, K is the number of modes, ∂_t is the time derivative, $\delta(t)$ is the dirac delta function, j is the complex unit ($j^2 = -1$), * is the convolution operation, $e^{-\mathrm{j}\omega\mathrm{kt}}$ represents frequency shifting relative to the center frequency of the mode and $\sum_{k=1}^{K} u_k(t)$ is the sum of all modes.

The point that should be particularly noted is that, through to the use of Lagrangian Mutipliers, the constrained optimization problem is transformed into an unconstrained problem and the solution is made more effective. In the VMD methodology, this mathematical formulation forms the theoretical basis of the signal decomposition process and yields powerful results in practice. In its basic formulation, VMD aims to decompose a signal into IMFs localized in different frequency bands. Here, the analytical signal is created using the Hilbert transform and the band-limited feature of each mode is tried to be preserved. This optimization problem is solved using the ADMM (Alternating Direction Method of Multipliers) algorithm and the modes are obtained iteratively. Unlike EMD, VMD separates all modes simultaneously and minimizes the mode mixing problem as shown by Figure 2.3.

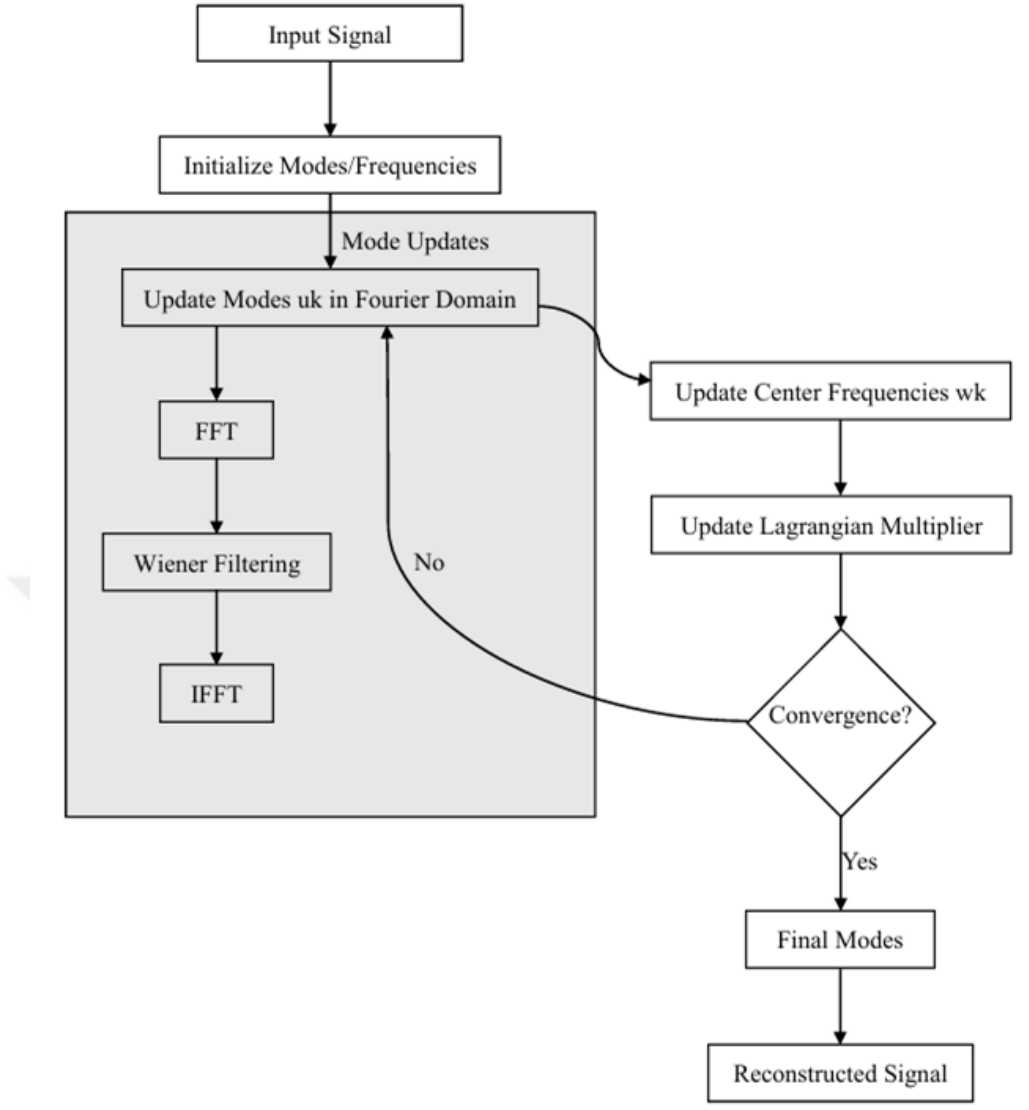

Figure 2.3 The VMD algorithm

2.3.2 Varieties of Variational Mode Decompositon

It has been observed that traditional VMD is limited in some applications or specific signal types, and therefore various variants have been developed as shown by Table 2.4. The type needed depends on the nature of the signal (e.g., energy density, complexity, noise level) and the purpose of the application.

The strong mathematical foundation of the original VMD is preserved in the variants. VMD and its variants provide better mode separation than EMD. The advantages are that the simultaneous mode extraction and optimization framework is well defined.

Table 2.4 Variants of VMD's, and their purposes and advantages

Main Variants	Purpose	Advantage
Multivariate VMD (MVMD) [22]	Simultaneous processing of more than one of the relevant signals, the continuity of the relationships between different channels and the extraction of common modes of multiple signals.	It provides more consistent separation between channels and preserves correlations better. The computational cost is lower compared to channels processed separately. It processes multi-channel data better.
Adaptive VMD (AVMD) [31]	Eliminating manual mode selection, and automatic optimization of parameters and adaptation to signal characteristics.	It reduced user intervention. It provides stronger performance across different signals. It has higher accuracy in mode extraction.
Robust VMD (RVMD) [32]	Increasing performance in noisy environments, handling outliers and impulsing noise, and it aims to increase decomposition stability.	It provides better noise resistance with its improved signal-to-noise ratio. Provides more stable mode extraction. Its performance is better with corrupted data.
Complex VMD (CVMD) [33]	Handling complex-valued signals, analyzing amplitude and phase simultaneously while preserving phase information.	It directs processing of complex signals, analysis phase better. CVMD completes signal characterization more and suitable for analytic signals.

Table 2.4 Variants of VMD's, and their purposes and advantages (continued…)

Main Variants	Purpose	Advantage
Weighted VMD (WVMD) [34]	Controlling the importance of different frequency components, focusing on specific frequency bands and customizing decomposition for specific applications.	It has better control over mod extraction. Provides improved performance for targeted frequencies. Allows more flexible parsing and application-specific optimization.
Fractional VMD (FVMD) [35]	Managing non-integer sorting systems. improving feature extraction and aims to better represent fractional order processes.	Better processing of fractional order dynamics, extraction of improved features to make the representation of certain physical processes more accurate and enables broader analysis of complex systems.
Multiscale VMD (MSVMD) [36]	Analyzing signals at multiple scales, improving frequency resolution and addressing multi-scale events.	It provides better processing of multi-scale signals and improved frequency separation. Better represents complex temporal structures.
2D VMD [37]	Processing spatial and spatial-temporal data, handling multidimensional signals and analyzing images and volumes.	Suitable for image processing Can manage spatial relationships. It is a better method for multidimensional data analysis. It protects spatial structures.

3
AIRCRAFT TOUCHDOWN DETECTION

3.1 Introduction and Problem Definition

In the first chapter of the study, the hardware differences of commercial aircraft, military aircraft and general-purpose civil aircraft were mentioned. Regardless of an aircraft's equipment level and field of use, it has two basic operational modes. One of these is the air mode in which the aircraft flies, and the other is the ground mode in which the aircraft is on its landing gear. In these two different operating areas, there are differences in many systems such as the forces acting on the aircraft, effective control surfaces and even the navigation systems used. Therefore, it is of great importance to accurately detect and process the mode changes that cause such a change in the general condition and use of the aircraft.

Considering the aircraft's air and ground operating modes, the transition between them can generally occur in two different ways. The first way to switch is from ground mode to air mode. This mode transition occurs when the landing gear is removed from the ground after the aircraft's takeoff run. Thus, the flight of the plane begins. Another mode transition is from air mode to ground mode. Transition to ground mode occurs with the Peel maneuver, in which the main landing gear touches the ground during the landing of the aircraft. It can be assumed that from this moment the aircraft began to operate in ground mode According to the data of the European Union Aviation Safety Agency (EASA) dated February 3, 2021, %44.05 of the accidents and crashes reported for general aviation aircraft between 2009 and 2019 occurred in the landing phase of the flight [38]. This renders the landing phase as the flight phase during which most accidents occur.

The aircraft's transitions between air and ground modes are both bidirectional and essential. On the other hand, the main goal in this part of the study is to ensure that

general aviation vehicles with hardware disadvantages can have a safe operating process in a low-cost manner. Therefore, within the scope of this study, the transition to ground mode will be specifically discussed. In this context, it can be put forward that if the situational awareness of the aircraft's transition to ground mode is provided to the pilot in manned systems and to the autopilot in unmanned systems, the accidents occurring during the descent phase may decrease proportionally. For this, the exact moment when the plane touched the ground must be known.

When studies on ground contact detection of aircraft are examined in the literature, it is seen that systems with strain gauge-derived sensors are generally used for detection purposes [39], [40]. Special sensors designed for this purpose can be found in the landing gear systems of high-tech military aircraft, large transport aircraft, new generation commercial aircraft or luxury private jets. With these sensors, data such as the load on the landing gear or the landing gear displacement can be measured and comments can be made about whether the aircraft has switched to ground mode. Although this method is capable of providing an accurate measurement for transition to ground mode, it introduces mechanical design challenges and extra cost in landing gear systems.

However, it is seen that approaches to detecting the ground contact point in relatively low-cost small aircraft with fewer sensors and equipment are generally carried out through data (position, speed, etc.) obtained through GNSS (Global Navigation Satellite System) receivers. Although the aircraft's ground contact area and approximate contact time can be calculated with these approaches, it is not always possible to accurately indicate the moment of contact [41], [42]. Factors such as the location errors of satellite-based data collection devices, which can exceed 25-30 meters in civilian use, the amount of errors accumulated by estimator algorithms, and the decrease in data quality of various external jammers, can be considered as limiting factors here [43].

Looking at other studies for contact detection, Jeong et al. by [44] there is an approach that works on an artificial neural network that can estimate the strains and loads on the landing gear and through which they detect contact. Mejias et al. [45] in another study by Lidar sensors and image-based approaches were used to detect ground contact. Although image-based approaches can provide suitable results in

laboratory environments, they can still be considered experimental approaches for real-world conditions due to both current camera technology and costs and weather conditions. Another approach used to detect the moment of contact is based on the analysis of speed and acceleration data that can be monitored in all aircraft using the Continuous Wavelet Transform (CWT) method [46], [47].

In this part of the study, all approaches in the literature are evaluated and the aim is to perform aircraft contact detection with a low-budget method that does not require high processing capacity. The motivations of the study are to accurately report the aircraft's transition to ground mode upon contact with the ground and to provide accurate time information for calculations that can be interpreted with the hardness of the landing. By notifying the aircraft of its transition to ground mode, an improvement is expected that will reduce accidents during landing by increasing awareness for both the pilot and the autopilot systems. By providing input into the calculations regarding the hardness of the landing and by maintaining the landing gear at the right times, it is aimed to prevent accident and destruction scenarios that may occur.

3.2 Application

In this part of the study, what data will be used to detect the aircraft's ground contact and the idea behind selecting these data will be discussed. Then, the transformations and operations to be applied on the selected data will be discussed.

3.2.1 Selection of Data to be Processed

As explained in the previous sections, the developed solution is aimed to be easily integrated into all classes of aircraft and to be low-cost. For this reason, Inertial Measurement Unit (IMU) was chosen to be used as the sensor.

Inertial measurement units (IMU) are sensors used to collect data in many different applications in aviation, space, automotive, robotics, wearable technology, mobile devices, and many other fields of industry. It is possible to find IMUs in a wide range of prices, from a few dollars to several hundred thousand dollars, depending on their areas of use, sensitivity levels, and mechanical and electronic strength features. At a fundamental level, it can be assumed that an IMU provides acceleration data in three axes and angular velocity data in three axes.

In the previous heading, it was mentioned that in this part of the study, the descent phase of the flight will be examined, together with the reasons. Looking at the internationally accepted landing protocols for an aircraft, the process to be encountered is as follows. First, the aircraft makes its final approach to land on the runway. It increases the angle of attack by performing the flare maneuver a certain distance from the ground. With this maneuver, the aircraft reduces its speed while at the same time obtaining the correct stopping angle for contact with the runway. It then puts the main landing gear on the runway and then lowers the nose, bringing all of its wheels into contact with the ground.

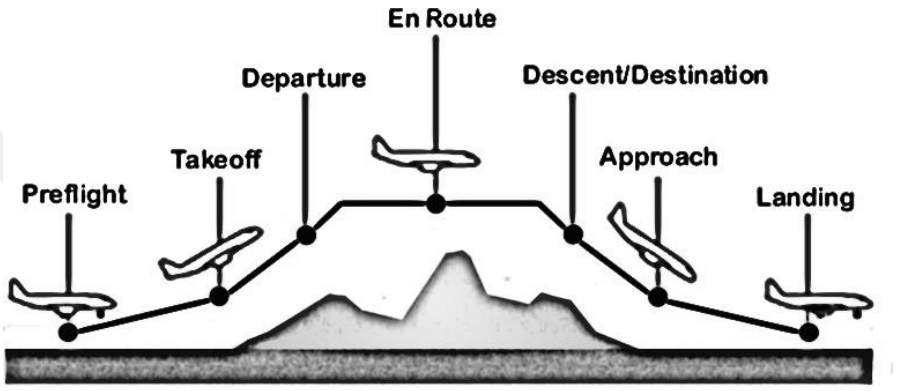

Figure 3.1 Flight profile for aircraft

All the main flight phases for a general aviation aircraft, from takeoff to landing, are given in Figure 3.1. From the perspective of physics at the landing event of the aircraft, it is a moving mass with 6 degrees of freedom. Aircraft can move in different axes during an ordinary landing due to the effects of many phenomena and external disturbances. However, since it is not possible to guarantee that these effects will occur in every situation, they cannot create observable movement patterns in every landing. The descent phase will be examined under ideal conditions, ignoring all external effects in order to ensure that the examination remains valid in more scenarios.

Under ideal conditions, the landing maneuver can be described as the resultant of the aircraft's movement in three axes defined in the body axis set. These are the translational movement in the x and z axes and the pitching movement, which is the rotational movement around the y axis.

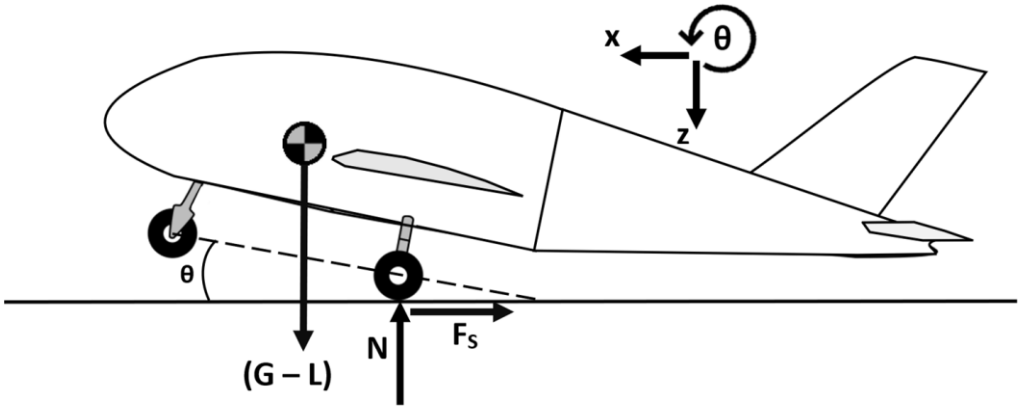

Figure 3.2 Ground-aircraft interaction at the moment the aircraft's first touchdown

During contact with the ground, in addition to the forces acting during the landing maneuver, forces arising from the interaction with the ground also affect the aircraft. The forces acting on the aircraft at the moment of first contact are given in Figure 3.2. Here, G refers to the weight of the aircraft due to gravity, L refers to the carrying force of the aircraft due to the wings, N refers to the reaction force applied to the aircraft by the ground, and F_S refers to the friction force between the tires and the ground, which are not yet rotating. Pitch angle, which is the angle the nose of the aircraft makes with the ground, is expressed as θ.

The aircraft absorbs the force coming from the ground with the rear landing gear, which is the first area in contact with the ground. Even if the G and L forces were somehow balanced during the time the air was present, the N and F_S forces acting on the system upon contact cause the balance to be disrupted. When the mass of the aircraft is assumed to be constant at the moment of contact with the ground, the newly added forces to the system cause acceleration changes in the x and z axes they act on. The acceleration relationship due to force and mass is shown by Equation (3.1). Here F represents force, m represents mass, and a represents linear acceleration. In this way, the motion effects in the x and z axes are explained.

$$F = m \cdot a \tag{3.1}$$

Another movement of the aircraft that needs to be examined is its rotational movement around the y-axis. In a standard airplane, the center of gravity is above the wheels. This situation causes a torque effect centered on the rear wheels, which

are stationary at the moment of initial contact and act as support points in the areas in contact with the ground. When the moment of inertia of the aircraft at the moment of contact with the ground is assumed to be constant, the newly added torque to the system causes angular acceleration change around the y-axis. The angular acceleration relation due to torque and moment of inertia is shown by equation (3.2). Here τ is the torque, I is the moment of inertia of the aircraft, and α is the angular acceleration. Thus, the effect of rotational movement around the y-axis is also explained.

$$\tau = I \cdot \alpha \tag{3.2}$$

Considering that the aircraft moves in 3 degrees of freedom, it can be said that ground contact can be detected theoretically only by examining the acceleration changes in these three axes.

It is apperant that fundamentally two forces are applied from the ground to the plane. The first of these is the normal force resulting from G and L forces. This force is the main cause of the linear acceleration change in the z axis. When different landings and landing data are examined, it is seen that soft landings can be achieved by keeping the acceleration change in the z-axis at levels that can be encountered in any part of the flight. This may vary depending on the pilot/autopilot's ability in the landing maneuver, the slope of the runway and the physical characteristics of the landing gear. Another force encountered during landing is the friction force resulting from the contact of the tires and the ground. Due to the mechanical structure of the aircraft and the offset between the center of gravity and the place where the force is applied, this force causes changes in two different accelerations. These are the linear acceleration on the x-axis and the angular acceleration on the y-axis. Friction force depends on the friction force between the ground and the tires and the weight on the wheel. Since large changes in these two components cannot occur with different landing maneuvers of the pilot/autopilot, acceleration changes due to friction force can be considered more stable and reliable.

In this case, ground contact detection can be properly performed by examining only 2 of the 3 degrees of freedom motion (linear motion in the x-axis and rotational motion in the y-axis). Hereby, the required processing capacity will be reduced as

the number of data to be examined will be reduced. It has been showen before that acceleration in three axes and angular velocity measurements in three axes can be obtained from a standard IMU. Thus situayed, among the six measurable data, the linear acceleration data on the x-axis will be taken and used directly, while the derivative of the angular velocity data on the y-axis will be used.

3.2.2 Transformations and Operations to be Applied to Selected Data

As explained with the reasons in the previous section, the data chosen to be used to determine the aircraft's ground contact are the linear acceleration on the x-axis and the angular acceleration on the y-axis. These selected datas are measurable quantities that vary contingent upon on time-dependent movement of the aircraft. The aim of the study is to detect the moment of ground contact, which cannot be measured directly with the specified aircraft and sensor configuration. In this case, measurable signals must be used to obtain unmeasurable target data by going through various processes. This situation is called virtual perception.

In order to determine which processes the signals will be subjected to in virtual sensing, if they are first evaluated in terms of the types of acceleration and angular velocity signals that we can measure with the IMU sensor of an aircraft, they can be classified as non-stationary and non-linear signals. The reason for this is that the aircraft in flight makes various and variable movements in line with its mission and flight purpose, and is exposed to different vibrations due to the aircraft's on-board equipment and external distortions.

As discussed in Chapter 2, the signal processing methods were evaluated in terms of their advantages and disadvantages based on the type of signal to be processed. Since the signals to be examined here may contain different frequency components at different times, they are classified as non-stationary signals and the Fourier transform method is not suitable for these signals. In this case, it is a more appropriate option to use CWT, which can provide better results in the analysis of signals with non-stationary and fast transitions.

Considering the moment the aircraft touches the ground; a sudden impact occurs on the fuselage and all parts. The body and structural elements under impact often have different vibration and frequency modes. This means that the ground contact phenomenon can be observed in a wide frequency band and within a certain time

interval due to different damping times. Although the frequency band is relatively wide, taking into account vibrations in unwanted regions requires the use of different sensors and requires more processing capacity. Therefore, EMD will be applied in addition to CWT to the signals to be examined for ground contact detection. The signals to be examined will be subjected to EMD process to separate unwanted frequency components and parts that disrupt linearity. Thus, the examined signal will be subjected to a kind of linearization process and will be prepared for CWT use. Then, by applying CWT to a mode selected from the EMD process outputs, the similarity of the processed signal to the template wavelet will be examined and the contact moment will be determined.

3.3 Test and Results

Until this part of the third chapter, the problem, planning and methods were mentioned and the selection processes for each were discussed. In this section, data collection, testing and simulation activities for aircraft ground contact detection will be explained. The results and graphics obtained from the bee will be presented.

The flight data to be collected within the scope of the study was obtained through the simulation program called X-Plane 11. X-Plane is a flight simulator first released in 1995 by production company Laminar Research [48]. X-Plane 11, the version used in the study, was introduced in 2016.

Flight tests were carried out at Tekirdağ Çorlu Airport with the code TEQ. A Cessna-172SP aircraft, one of the most used civil aviation models, was used for the flight. Flight data was recorded with a frequency of 40 Hz. Since acceleration data cannot be obtained directly from the simulation, the acceleration data to be processed was obtained by taking the derivatives of the relevant angular and linear velocities. The graphic of an example flight selected from many flights is given in

Figure **3.3**. The stall event in flight and the moment the aircraft touches the ground are marked and shown in the graphics.

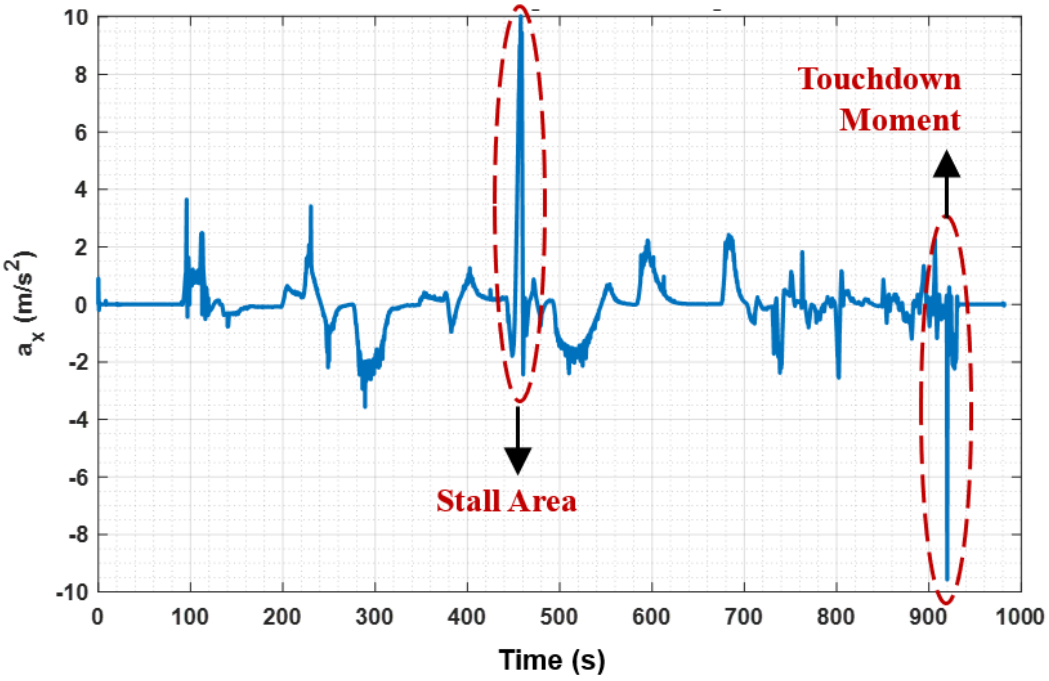

Figure 3.3 X-Axis linear acceleration graph of the sample flight

All flight data can be seen in the graphics given in Figure 3.4 and Figure 3.5. In the graph given in Figure 3.4 CWT was applied directly to the raw data and Morlet wavelet was used as the wavelet function. In the graph given in Figure 3.5, EMD process was first applied to the raw data, and CWT was applied to the first of the IMFs obtained in this process.

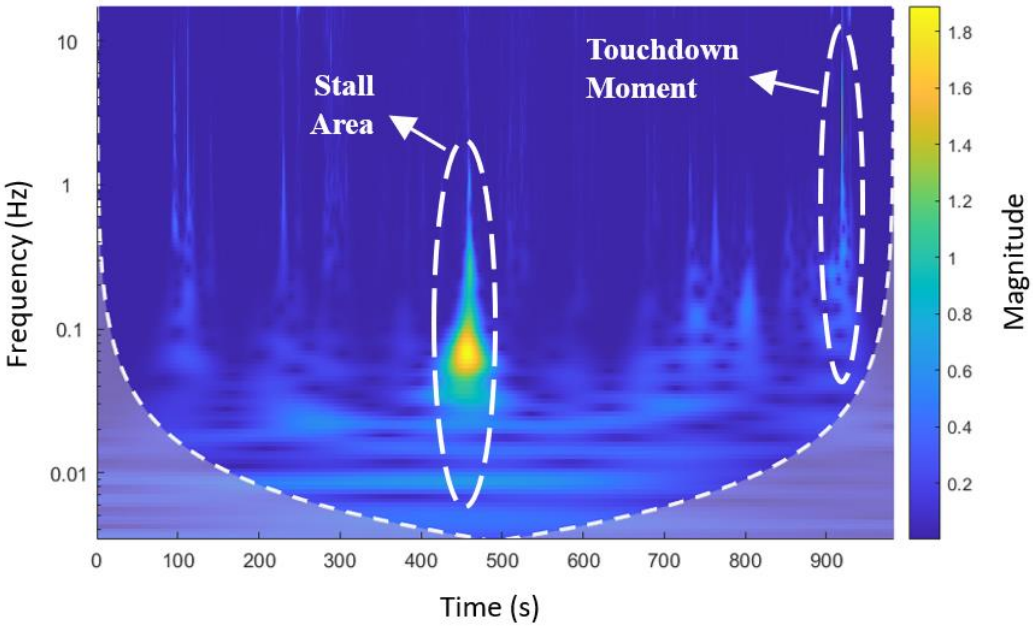

Figure 3.4 X-Axis linear acceleration CWT scalogram

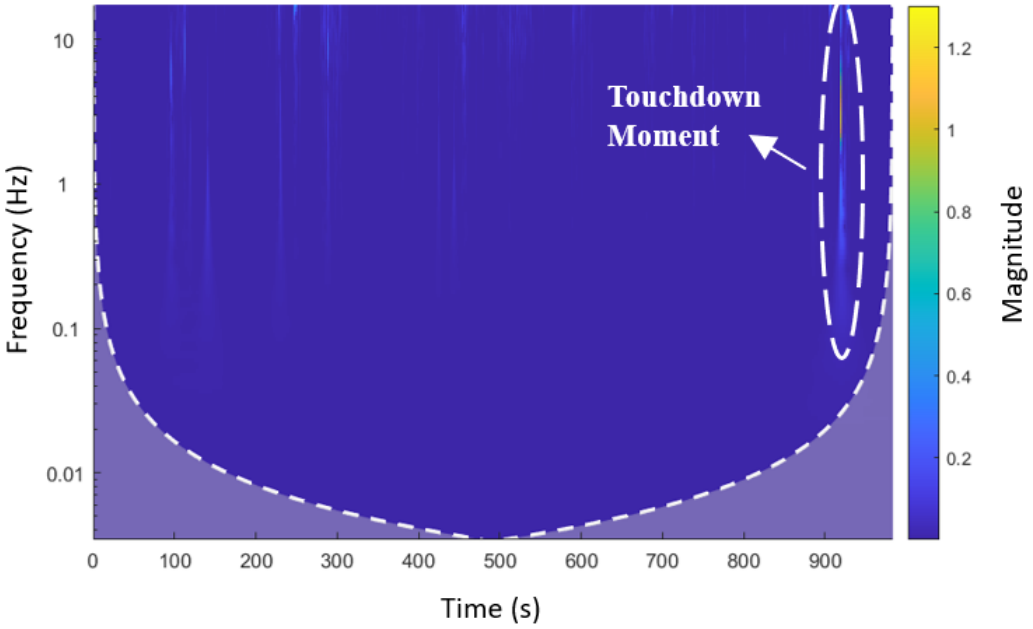

Figure 3.5 X-Axis linear acceleration EMD IMF-1 / CWT scalogram

3.4 Conclusion

In the previous section, test conditions were mentioned and result graphs were given. In the linear acceleration on the x-axis, the landing zone is visible and marked in the graphs of each technique. However, in a scenario where the landing zone is expected to be determined by automatic algorithms, ensuring that the moment of contact with the ground is separated from other regions as much as possible will directly affect the accuracy and development process of the algorithm.

Particularly when looking at all the flight graphics given in Figure 3.4 ve Figure 3.5, the difference between applying CWT directly and applying EMD first and then CWT is clearly seen. Applying first EMD and then CWT to the raw data largely eliminated unwanted frequency effects. In fact, even the stall event seen in the graph given in Figure 3.4, which can be clearly separated from other regions in terms of magnitude, cannot be seen in the graph given in Figure 3.5.

In this case, it has been experimentally presented that if it is desired to detect ground contact using only IMU data with an automatic detection algorithm, the most appropriate of the two techniques will be the recommended method.

One of the factors limiting the research in this study is the data recording frequency of 40 Hz. Although the ground contact phenomenon can be visualized in the studied

area, whether there are other components at higher frequencies is an issue that remains open in the study.

One of the future studies for this study will be to create an automatic algorithm that detects ground contact from the virtual detection results obtained by processing IMU data. In addition, the study should be tested on different aircraft with the same method and it should be questioned whether there are parameters that need to change from aircraft to aircraft for the algorithm. With all things considered, it is an undeniable need to verify the resulting algorithm by testing it in real systems other than simulation.

4
TURBULANCE DETECTION AND AIRCRAFT SPEED LIMITATION

4.1 Introduction and Problem Definition

In previous sections, the disadvantages of relatively low-budget general aviation aircraft in terms of equipment and technology level were mentioned. It was also announced that each aircraft has two different modes: ground mode and air mode. In this part of the study, the turbulence event that the aircraft will encounter while in air mode, the detection of the turbulence event and the recommended action to reduce its effects will be discussed.

Turbulence can be defined as the irregular and chaotic flow of any fluid. The main thing that allows aircrafts to hang in the sky and fly is the air in the atmosphere. Air is a gas mixture consisting of nitrogen, oxygen, carbon dioxide and some other gases in small percentage amounts. Since it is a gas, it is in the class of fluids. Turbulence occurring within air masses disrupts the flow on the fuselage and wings of an aircraft passing there. This flow disturbance leads to unpredictable load variations and undesired motion perturbations on the aircraft.

According to a report published by the Federal Administration Aviation (FAA) in 2016 [49], there were 222 accidents caused by turbulence reported in the 12-year period between 2002 and 2013. Forty-seven percent of these cases are caused by general aviation aircraft grouped as "Part 91". Among the turbulence incidents, 89% of the accidents causing fatal injuries were reported by general aviation aircraft. When the statistics are examined, the aircraft group that has the highest and most severe weather events described as turbulence are general aviation aircraft. For this reason, the second situation chosen to be examined in this study aimed at increasing situational awareness in the use of general aviation aircraft is turbulence.

The turbulence phenomenon is examined under the general heading of weather events. There are multiple situations that can cause turbulence that aircraft may be exposed to. These conditions can be classified into four fundamental categories. The first of these is turbulence caused by surface shapes. Natural landforms or human-made structures that disrupt air flow cause turbulence. In the second category, there is a type of turbulence called Clear Air Turbulence (CAT). CAT events are generally occur from jet streams, which are atmospheric air currents, and cannot be predicted by the eye. The third category is turbulence caused by the engines and wingtip flows of other (and often larger) aircraft. The fourth and last category is the temperature distribution imbalances on the earth due to various reasons. Temperature differences create temperature variations between air masses that come into contact with the corresponding regions of the earth's surface. As a result, shifting hot-cold air masses cause unpredictable air flows and tubulence.

These turbulence events, which are divided into four categories, are valid for all general aviation aircraft and even all aircraft. On the other hand, fire-fighting aircraft are among the aircraft that are most likely to fall into all four categories and have to encounter turbulence most frequently. Therefore, the turbulence problem will be evaluated in terms of airtankers classified as general aviation aircraft.

In this chapter of the study, it is aimed to determine the turbulence severity experienced by general aviation aircraft, specifically airtanker, with a low-budget and effective method. For this, data measured from the IMU Sensor will be used and the severity of turbulence on the aircraft will be determined by the virtual detection method. Then, a minimum IAS recommendation will be made to the pilot or autopilot system depending on the severity of turbulence the aircraft is exposed to.

4.2 Application

In this part of the study, the basic information that needs to be known in order to better understand and solve the determined problem will be given. Then, the selection of the data to be examined in order to determine the turbulence intensity, the reasons for the selection, how this data will be collected and how it will be processed will be discussed. Then, the system designs related to the measurement

of turbulence intensity and the determination of the minimum air speed suitable for flight for the aircraft will be discussed and the design steps will be explained.

4.2.1 The Turbulence

In this heading of the study, the definition of the turbulence phenomenon, its types, and its effects on aircraft will be discussed.

Turbulence is the name given to the situation where a fluid continues its flow with irregular, unpredictable, and chaotic vortex movements instead of a linear and regular flow. Turbulence can occur in any fluid due to various reasons. The air around aircraft is also a gas and therefore a fluid. This means that aircraft can be exposed to turbulent effects during their flights.

Turbulence can be examined in four basic subcategories depending on the conditions and reasons for its formation. The first category is called Clear Air Turbulence (CAT). CAT is a type of turbulence that occurs suddenly without any visible meteorological indicators in the sky. It is one of the most challenging types of turbulence for aircraft because it is difficult for pilots and air control stations to predict.

The second category is called Wake Turbulence. This type of turbulence is caused by vortices formed on the wing tips and engine exits of aircraft. Especially aircraft that have to land and take off repeatedly at airports are likely to encounter this type of turbulence. Since this type of turbulence does not contain enough energy to move very large air masses, it is relatively ineffective against large aircraft. On the other hand, it has the potential to create situations that can have major effects on general aviation aircraft with relatively low masses.

The third category is called Mechanical Turbulence. Mechanical turbulence occurs as a result of the disrupted flow of air masses when they encounter large ground objects such as mountains. It can create sudden and unexpected effects, especially for aircraft that must fly in mountainous terrain or in valleys.

The fourth and last category is called Thermal Turbulence. Thermal turbulence is based on convective causes caused by the rising air masses, which are heated due to different temperature levels on the earth's crust, and the rising air masses are filled with colder air masses. Shifting warm-cold air masses cause unpredictable air

flows and the formation of turbulence. It can have serious effects on aircraft, especially in flights close to the ground.

Turbulence is an important atmospheric phenomenon in terms of flight safety of aircraft. Since turbulence is directly related to the air masses in which the aircraft is located, every movement of the air mass is also reflected in the aircraft. Flight comfort may decrease in aircraft that encounter various flows and vortices, and the pilot may experience short-term loss of control over the aircraft. In scenarios where turbulence intensity is very high, air masses affecting from different angles may create unexpected loads on aircraft and can cause structural damage.

4.2.2 Airtankers

In this heading of the study, it will discuss airtankers, their duties and their types.

Airtankers are specialized aircraft used in important tasks such as fighting forest fires and disaster relief. Although there are larger airtankers classified in the military category, airtankers in general use are classified as general aviation aircraft.

Airtankers used for firefighting purposes are aircraft that carry various retardant and extinguishing liquids in their reserve tanks. They are used for aerial intervention in fires of various sizes, large and small, depending on the amount of liquid they can carry and the size of the aircraft. Firefighting aircraft are of critical importance, especially in large-scale fires that occur in nature. They can easily reach points that ground crews have difficulty reaching and can discharge large amounts of extinguishing liquid into the fire area at once. In addition, they have the ability to see the big picture of the fire incident in a way that air crews do not. This ability allows for shorter intervention times and for the fire to be brought under control in a shorter time. Figure 4.1 shows an airtanker emptying the retarder liquid from the reserve tank.

If firefighting aircraft are examined according to their types and models, it is possible to come across different models with a wide range of power and classes [50]. It is possible to examine airtankers under four main classes. The first of these is the Very Large Airtanker (VLAT) class. VLATs can carry over 40 tons of retardant liquid in their reserve tanks. VLATs are the largest airtanker class in terms of size among the four classes to be examined. The second class is the Large Airtanker class. Airtankers in this class have smaller dimensions than VLATs.

Thus, they have an advantage in terms of maneuverability. They can carry up to 18 tons of retardant liquid in their reserve tanks. The third class is the Water Scoopers class. These aircraft are amphibious aircraft that have the ability to fill their reserve tanks with liquid from sources such as lakes and rivers on the surface of the earth. Water scoopers come in various sizes and there are types that can carry up to 7 tons of liquid. The fourth and final class is the Single Engine Airtanker (SEAT) class.

Figure 4.1 Illustration of an airtanker emptying the retardant liquid from its reserve tank

One of the most popular models of the SEAT class aircraft is the Air Tractor AT-802 model firefighting aircraft, which is used by many countries around the world. The AT-802 is an aircraft classified as a single engine air tanker (SEAT). The first model of the AT-802 flew in 1990. With an empty weight of 2900 kg and a maximum take-off weight of 7000 kg, the AT-802 has the ability to carry nearly 3 tons of retardant and extinguishing liquid. The AT-802, which has a wingspan of 18 meters, is powered by a 1350 hp PT6A class engine [51].

SEAT class aircraft have the ability to serve in a wide variety of terrain conditions with their high maneuverability and relatively small size. During firefighting, this type of aircraft flies over landforms at a height of 20 to 45 meters and discharges the fire retardant in reserve tanks into the fire area. As the distance of the aircraft from the ground increases, the contact of the fire retardant to the targeted area decreases. Additionally, the aircraft needs to reduce its speed to the minimum possible level during the discharge of fire retardant. Flying the aircraft at low speeds ensures that the fire-retardant falls vertically to the ground in the form of raindrops and reaches as much area as possible, covering the ground. As the flight speed

increases, the angle at which the liquid falls to the ground decreases, causing a phenomenon called shadowing. Shading causes the fire retardant to not be able to pass behind trees, bushes, and similar objects, leaving gaps on the ground. As a result, the fire continues to be effective in spaces where the fire retardant cannot reach.

Airtankers should fly as low as possible and at as slow speeds as possible in order to discharge the fire retardant to the target area with higher accuracy and to avoid the shadowing effect. This makes aircraft vulnerable to turbulence effects caused by both surface shapes and high temperature differences.

4.2.3 Selection of Data to be Processed

In this heading of the study, the selection of parameters that need to be processed in order to solve the problem, achieve the goals and answer the research question will be discussed.

In the previous section, what SEAT class airtankers encountered during a firefighting mission and their flight behavior during firefighting were mentioned. Drawing from what was explained, it can be said that the two most important criteria during a SEAT's mission flight are to fly low and slow. If this targeted flight style is examined in terms of flight physics, it should start with the ability of an aircraft to stay in the air.

In order for an aircraft to fly, it must produce lift force. Aircraft produce the carrying force that enables them to stay in the air through the air flowing over their wings and body. The air that comes into contact with the leading edge of the wings moves in a regular flow along the surface of the wing and reaches the trailing edge. As the air leaves the wing from the trailin edge, it continues on its way with a downward flow due to the shape of the wing. As a result of directing the air mass in this way, a lift force is created that pushes the wing upwards, in the opposite direction of the movement of the air mass.

In order for an aircraft to fly at a constant altitude, it must produce a lifting force equal to its own weight. There are many factors on which this lifting force depends, and the most fundemental is airspeed. Airspeed refers to the relative speed of an aircraft with respect to the air mass in which it is located. When the airspeed of an aircraft flying at a fixed altitude and with fixed stance angles increases, the lift force

increases and this causes the aircraft to rise. On the contrary, the decrease in airspeed during a flight at constant altitude and constant stance angles also leads to a decrease in lift force. As the carrying capacity decreases, the aircraft becomes unable to support its own weight and begins to descend, unable to maintain its altitude. This situation is called “stall.”

$$L = \frac{1}{2} \cdot \rho \cdot v^2 \cdot C_l \cdot A \tag{4.1}$$

The general equation of the lift force is given in Equation (4.1). Here, L is the lift force (Newton), ρ is the air density (kg/m^2), v is the airspeed (m/s), A is the wing area (m^2) and C_l is the lift coefficient. Lift coefficient, in its most fundemental form, is a constant and unitless coefficient formed depending on the interaction of the air mass with the wings.

$$L = W \tag{4.2}$$

If the equation given in Equation (4.2) is substitued into Equation (4.1), Equation (4.3) is obtained, from which the stall speed of the aircraft can be calculated.

$$v_{stall} = \sqrt{\frac{W}{\frac{1}{2} \cdot \rho \cdot C_l \cdot A}} \tag{4.3}$$

Here, v_{stall} indicates the minimum airspeed (m/s) at which the aircraft can carry its own weight and W indicates the weight of the aircraft (Newton).

When Equation (4.1) and Equation (4.3) are evaluated in terms of SEATs' flight requirements, a way must be found to keep the lift force constant while reducing the airspeed to speeds close to the stall speed. Considering the components contained in the equations, it has been seen that the parameters that can be changed instantly by pilot intervention are airspeed (v) and lift coefficient (C_l). All parameters other than these parameters depend on the environmental conditions and the physical condition and structural characteristics of the aircraft. Thus, in a situation where the airspeed must approach the stall speed as much as possible, manipulation of the lift coefficient stands out as the only way to keep the lift force constant. Lift coefficient consists of many subcomponents depending on the aircraft's attitude angles and surface commands.

Lift coefficient calculation is shown using some basic sub-components in Equation (4.4)

$$C_l = C_{l\_0} + C_{l\_\alpha} \cdot \alpha + C_{l_{da}} \cdot da + C_{l\_\beta} \cdot \beta + \cdots \quad (4.4)$$

Here, C_l is the lift coefficient, C_{l_0} is the main lift coefficient component resulting from the structural features of the wing and similar areas that produce the lift force, C_{l_α} is the lift coefficient component resulting from the angle of attack, α is the angle of attack (rad), C_{l_da} is the lift coefficient component resulting from the position of the aileron surface, da is the aileron surface position (rad), C_{l_β} is the lift coefficient component resulting from the slip angle of the aircraft, and β is the slip angle of the aircraft (rad). Three dots are used to indicate that there are other subcomponents that are not considered in the equation.

One of the most dominant components in the total lift coefficient calculation is the angle of attack component. In this case, increasing the angle of attack stands out as the most basic method of ensuring that the lift force of an aircraft whose airspeed is to be reduced remains constant and maintains its current altitude. Angle of attack is the name given to the angle between the aircraft's longitudinal reference axis and the air flow.

The variation of the C_{l_α} coefficient seen in Equation (4.4) is different for each aircraft. From a general perspective, as the angle of attack increases, the C_{l_α} coefficient increases up to a certain value, resulting in an increase in the lift force. After a certain threshold value, the bearing force suddenly decreases. As mentioned before, the lift force is generated by the flow of air over the wings. When the angle of attack of the wings exceeds a certain value, the air flow begins to break away from the wing surface. As the air flow breaks away from the wing surface, the air volume that can be used to create the lift force decreases and the laminar flow of the air mass is disrupted, causing a turbulent flow over the wing. This causes the aircraft to be unable to produce more lift force. As a result, the aircraft becomes unable to support itself, stalls and begins to lose altitude. For SEATs that perform mission flights at altitudes very close to the ground, stalling and altitude loss may have irreversible consequences. Based on all this, it can be said that the angle of attack is one of the most critical parameters for SEATs. For this reason, the first parameter chosen to be examined is the angle of attack.

$$\alpha = \theta + \gamma \tag{4.5}$$

Equation (4.5) gives the relationship between the fundemental angles affecting the longitudinal behavior of the aircraft. Here, θ denotes the pitch angle of the aircraft, γ denotes the climb angle defined in the body axis system of the aircraft, and α denotes the angle of attack.

The effect of turbulence in the air mass on an aircraft is basically modeled by angular and linear velocity changes. Irregularity of airflow causes unpredictable angular velocities to be induced on the aircraft and distortions in attitude angles. Depending on the severity of turbulence, these effects can cause large changes in stance angles. A possible change in pitch angle directly affects the aircraft's angle of attack and climb angle. In this case, while the change in the climb angle disrupts the altitude that the aircraft is trying to keep constant, the change in the angle of attack may cause the aircraft to exceed the stall limit.

The critical effects of turbulence on angle of attack and altitude change are discussed. In this case, considering the data measured with the IMU sensor selected as the data collection tool, the two most appropriate parameters are the acceleration in the z-axis and the angular velocity in the y-axis. While the aircraft's acceleration in the z-axis will show the effects of altitude change, its angular velocity in the y-axis will show the effects of the pitch angle. As discussed in Equation (4.5), the change in pitch angle includes both altitude changes and stall effects.

As a result, three parameters were selected to be examined as a result of all the effects considered. These are the parameters angle of attack, acceleration in the z-axis, and angular velocity in the y-axis, all of which can be obtained directly by processing IMU sensor data.

4.2.4 Procedures to be Applied to Selected Data

In this heading of the study, how to process the parameters selected to be examined in the previous heading will be discussed. The signal processing methods to be used in processing the parameters and the reasons behind choosing these methods will be discussed.

Due to the reasons explained in detail in the previous heading, the parameters chosen to be examined are angle of attack, linear acceleration in the z-axis, and

angular velocity in the y-axis. These data, which are selected to determine the level of turbulence affecting the aircraft, are measurable quantities that vary depending on the time-dependent movement of the aircraft. The aim of the study is to detect the turbulence intensity that cannot be measured directly with the specified aircraft and sensor configuration. In this case, the virtual detection method will be used, in which measurable signals are processed through various processes to obtain unmeasurable target data.

At this stage, the characteristics of the signal must first be examined to determine which processes the signals will be subjected to. If the parameters selected to be used in the study are evaluated in terms of signal types, they can be classified as non-stationary and non-linear signals. An aircraft that has taken off makes various and variable movements in line with its mission and flight purpose. In addition to these various maneuvers, different vibrations are also induced on the IMU sensors due to the aircraft's onboard equipment and external disturbances. For these reasons, static or linear IMU signals cannot be mentioned in an aircraft.

Recalling the signal processing methods mentioned in Chapter 2 of the study, advantages and disadvantages are mentioned depending on the type of signal to be processed. Since the signals to be examined here may contain different frequency components at different times, they are classified as non-stationary signals and the Fourier transform method is not suitable for these signals. In this case, it is a more appropriate option to use CWT, which can provide better results in the analysis of signals with non-stationary and fast transitions.

In addition to the CWT method, the EMD method, which has previously been shown to be effective for ground contact detection, will be used to separate unwanted frequency components from the signals to be examined. On the other hand, the effects of turbulence on the aircraft are seen on fewer components than at the moment of contact with the ground and occur in a narrower frequency band. For this reason, the VMD method, which is more resistant to mode interference, will be used in addition to the EMD method to separate unwanted frequency components.

The signals to be examined will first be decomposed into their modes by separately applying EMD and VMD processes. In this way, unwanted frequency components and parts that disrupt linearity will be separated and the examined signals will be

subjected to a kind of linearization process. Then, the appropriate modes will be determined, CWT will be applied to these modes, and the similarity of the processed signal to the template wavelet will be investigated. The obtained quantities will also be related to the severity of the effect of turbulence on the aircraft.

4.2.5 Data Collection and Analysis

In this heading, the process of collecting flight data regarding the parameters selected to be examined with the IMUs on the aircraft and the processing and analysis of these collected data will be discussed.

In order to carry out the entire application, data must be collected and analyzed by performing flight tests under various conditions. For this purpose, data can be collected by flying a real aircraft, or the data collection process can be furthered through flights in a simulation environment. At this point, the simulation environment was chosen to proceed. The reason for this is that the simulation environment has lower costs than real flight tests and can provide more isolated environments for controlled tests to be carried out.

Simulink environment, a product of Mathworks company, was preferred for simulation tests. A ready-made general aviation aircraft model in the Simulink environment was purchased and customizations were made on the aircraft model to make it resemble a SEAT. The SEAT model taken as an example to simulate the aircraft in the model is the Air Tractor AT-802. The physical dimensions of the aircraft in the model are matched to the AT-802. A turboprop engine that alone can provide 1600 hp was added to the aircraft. In its final state, the empty mass of this modeled aircraft was measured to be 3200 kg and the maximum take-off mass to be 7000 kg.

Von Karman turbulence model was used to add random wind and flow changes to the simulation environment. This model is able to simulate small and large eddies of the air mass with the help of a function called the wind spectrum. This allows high and low frequency turbulence effects to be realistically transferred to the simulation environment. The airspeeds taken as the output of the turbulence model were added to the aircraft as linear velocity and angular velocity, allowing the turbulence effect to be observed on the aircraft.

For the purpose of data collection, flights were carried out at many different altitudes and weather conditions, and various maneuvers were performed during the flights. One of these flights has been selected to be shown here. The selected example flight is a test flight performed under more controlled and isolated environmental conditions in order to directly demonstrate the effects of turbulence.

The sample flight to be examined was carried out in a windless environment and at ISA 0 temperature. The aircraft started its flight with a mass of 4050 kg and finished it with a mass of 3930 kg. Based on this, it can be said that the average mass during flight is 4000 kg. During the test, the aircraft flew at an altitude of 800 meters above ground level and a barometric altitude of 1000 meters. At the beginning of the test, the roll angle of the aircraft was trimmed to 3 degrees and it was allowed to fly on a circle line. In addition, considering the mission flights of a SEAT, the stall angle was made as close as possible to the angle of attack of 7 degrees, and it was allowed to fly at an angle of attack of 6 degrees. In the current environmental conditions for the aircraft used, an angle of attack of 6 degrees corresponds to an indicated air speed (IAS) of 41 m/s. In order to prevent pilot-related differences during the flight test, the aircraft's autopilot system was activated and the altitude and speed controllers were engaged. The autopilot was set to fly the aircraft trimmed at 1000 meters barometric altitude and 41 m/s IAS.

IAS and barometric altitude graphs for the sample flight are given in Figure 4.2 and Figure 4.3. The command values and measured values created for the autopilot are shown in the graphs.

In this flight, the aircraft flew in non-turbulent weather conditions from the 250^{th} to the 450^{th} seconds. Then, the turbulence model was activated and set to level 1 turbulence intensity, which is the lowest level. From this point on, the turbulence intensity was increased by one level every 150 seconds and the flight was continued. When the turbulence intensity was level 5, the autopilot's speed command had to be increased first to 42 m/s and then to 43 m/s in order for the aircraft to continue the flight without stalling. At the 1350^{th} second of the flight, level 7 turbulence, the most severe turbulence, started. Then, at the 1400^{th} second, the autopilot's IAS command began to be increased to observe the effects of turbulence according to the change in airspeed. When the aircraft reached its maximum speed of 80 m/s, the autopilot was commanded again to 41 m/s. At the

1700th second of the flight, the turbulence level was reduced from 7 to 1. After the aircraft flew with level 1 turbulence for 150 seconds, the turbulence was turned off at the 1850th second and the test was terminated at the 2000th second.

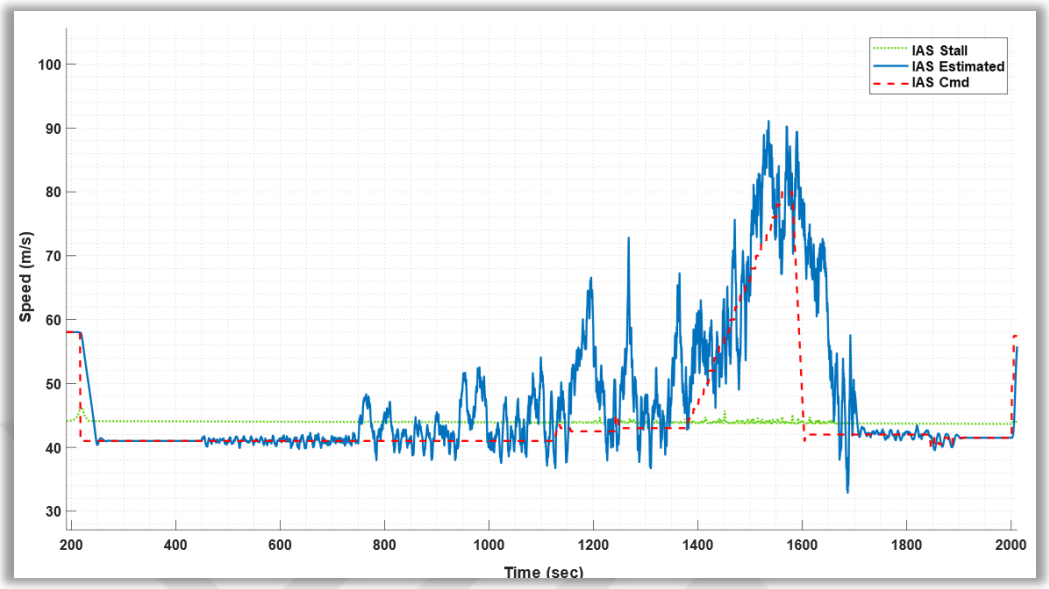

Figure 4.2 IAS graph for the example flight

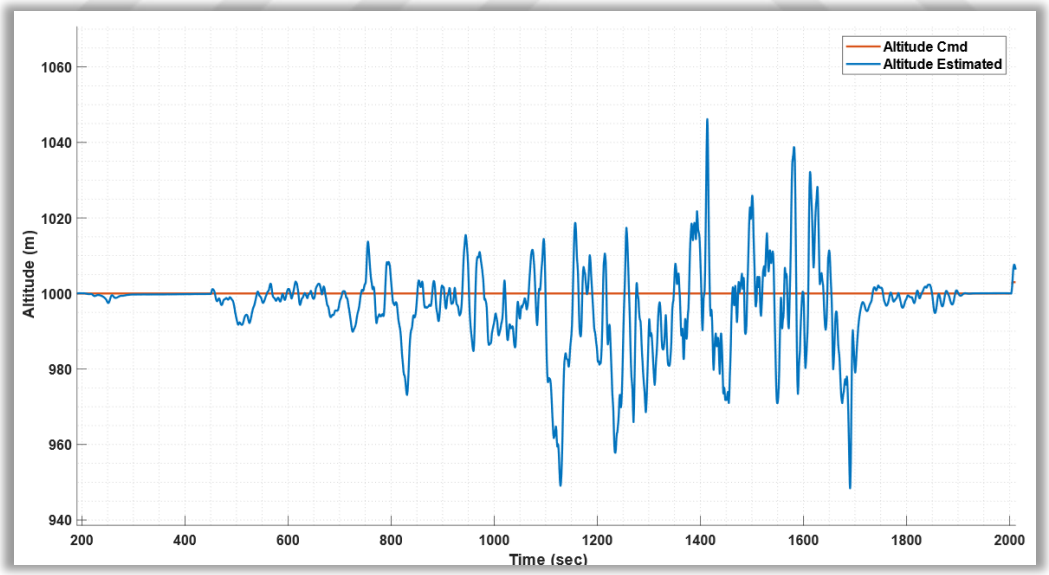

Figure 4.3 Barometric altitude graph for the example flight

Graphs of the IMU data measured in this sample flight are given in Figure 4.4, Figure 4.5 and Figure 4.6. The measurement frequency of the collected IMU data is 50 Hz. For each data, it is seen that the oscillation amplitudes increase as the

turbulence level increases. In these graphs drawn in the time domain, there is no visible clear effect of increasing IAS in level 7 turbulence.

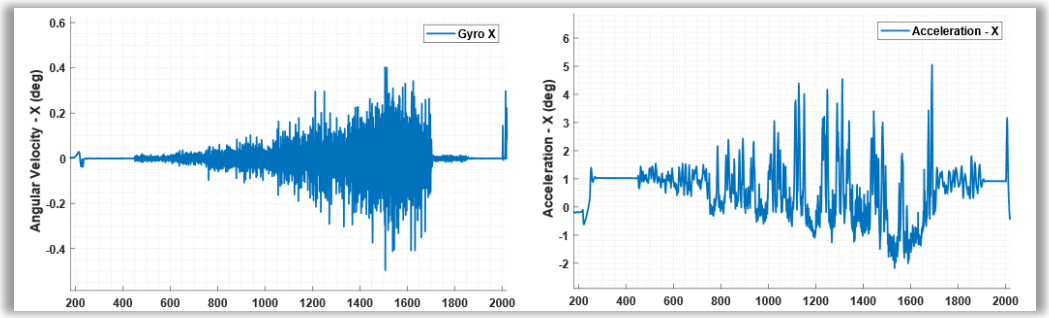

Figure 4.4 IMU measurements of x-axis angular velocity (left) and linear acceleration (right) for the sample flight

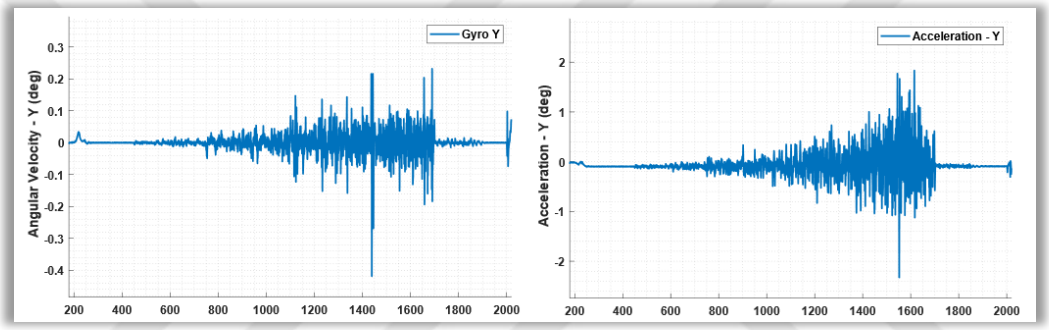

Figure 4.5 IMU measurements of y-axis angular velocity (left) and linear acceleration (right) for the sample flight

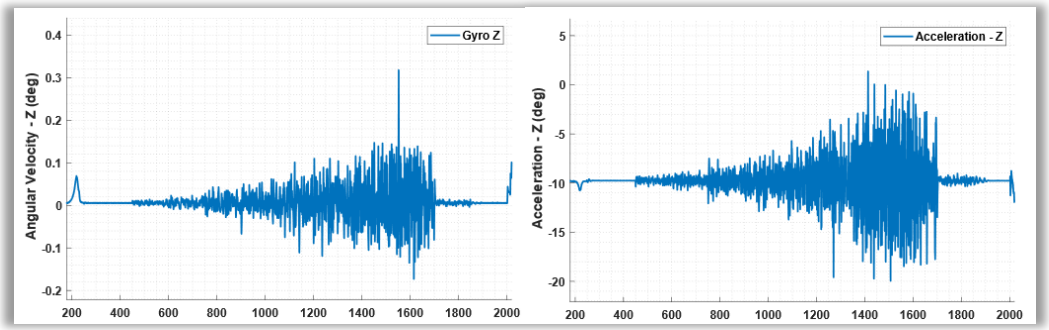

Figure 4.6 IMU measurements of z-axis angular velocity (left) and linear acceleration (right) for the sample flight

Following this data collection phase, the data processing phase was initiated. By taking the data previously selected for analysis, each of the three data was first subjected to the CWT process in its raw form. Morse wavelet was used for CWT process. The results of the graphs obtained for three data are given Figure 4.7, Figure 4.8 and Figure 4.9. Figure 4.7, Figure 4.8 and Figure 4.9 give the result

graphs obtained for the transformations of the three data.) When examining the graphs, it can be seen that the data contains components at various frequencies.

The graphs should be examined by considering the 0^{th} second of the time axis seen in the scalogram graphs and the 200^{th} second of the flight graphs given as far as being at the same point.

After examining the CWT results of the data, the proposed methods were implemented. As the first variation of the proposed methods, the data was started with the EMD process. EMD process was applied to a total of seven data collected from the flight, including 6 data collected with the IMU sensor and the angle of attack data obtained from these data. EMD was applied to the data at 3 different levels, limiting the maximum intrinsic mode function (IMF) numbers to be obtained at 5, 10 and 15. As a result of the application, it was observed that no data could be decomposed up to 15 IMF, and the decomposition iteration generally ended after 10-12 IMF. Then, the CWT process was applied separately to each of the EMD results with 10 IMFs and EMD results with 5 IMFs. When the result scalogram graphs were examined, it was concluded that the extra processing capacity allocated to obtain 10 IMF was unnecessary compared to the resulting performance.

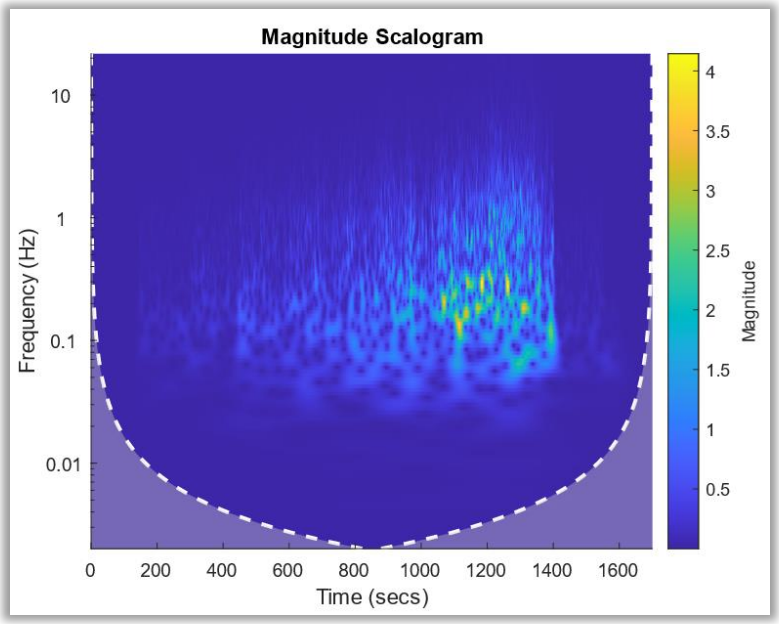

Figure 4.7 Magnitude scalogram obtained as a result of the CWT process for the z-axis linear acceleration data collected in the the sample flight

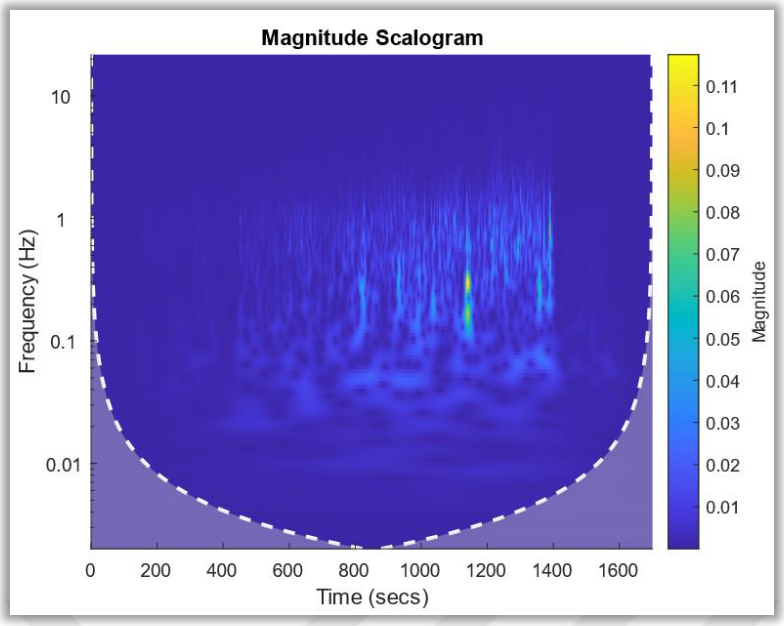

Figure 4.8 Magnitude scalogram obtained as a result of the CWT process for the y-axis angular velocity data collected from the sample flight

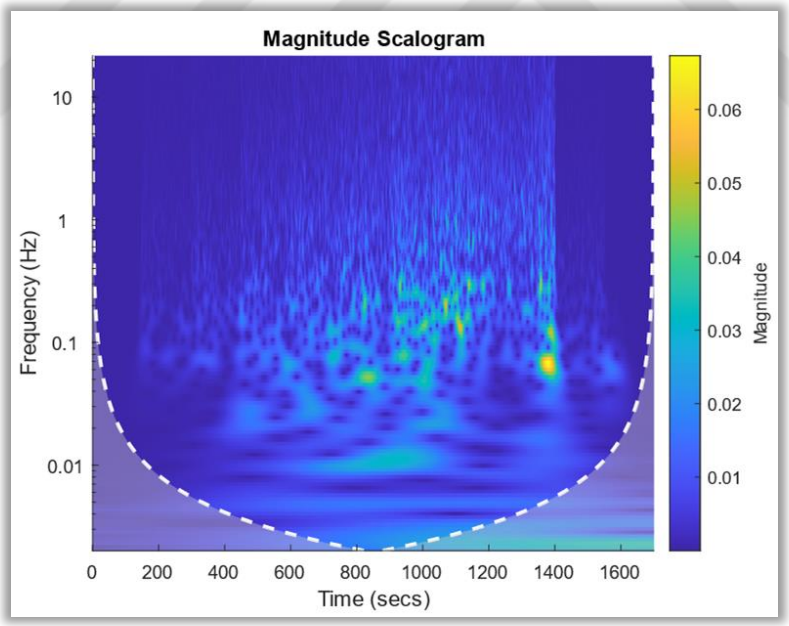

Figure 4.9 Magnitude scalogram obtained as a result of the CWT process for the angle of attack data collected from the sample flight

The performances of CWT conversion results were evaluated based on the change according to the turbulence level. Depending on the increase in turbulence level, the magnitudes in the scalogram graph were determined to increase steadily and at equal intervals as a selection criterion. As a result of the evaluations, three basic

conclusions were made. The first conclusion is that applying an EMD process with 5 IMF to the data will be sufficient. In this case, it was decided to use the EMD process with 5 IMFs for analysis in the following parts of the study. It is aimed that this decision will provide an advantage in terms of processing capacity and system requirements if the study is intended to be applied to embedded systems that will work in real time. The second conclusion drawn is that the three parameters determined to be examined in the previous sections were determined correctly. As a result of evaluating the seven parameters that were processed and analyzed according to the selected evaluation criteria, it was seen that the parameters with the highest potential for use were the three parameters chosen first. The third conclusion is that the most appropriate modes to use for detecting turbulence effects as a result of the 5 IMF EMD process are the second and third modes. While no change was observed depending on the turbulence level in some of the other modes, it was observed that in some of the other modes the results were distorted by effects from very different frequency levels.

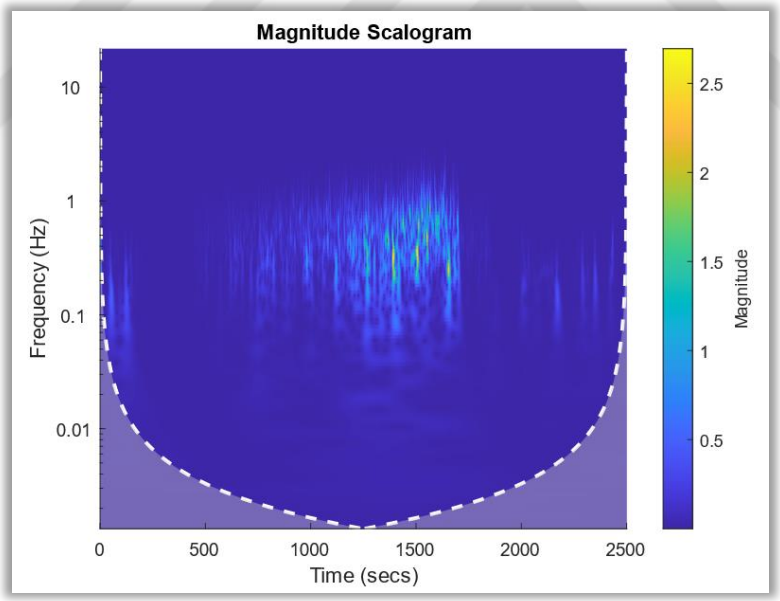

Figure 4.10 Magnitude scalogram obtained by applying EMD to the z-axis linear acceleration parameter and then applying CWT to IMF-3

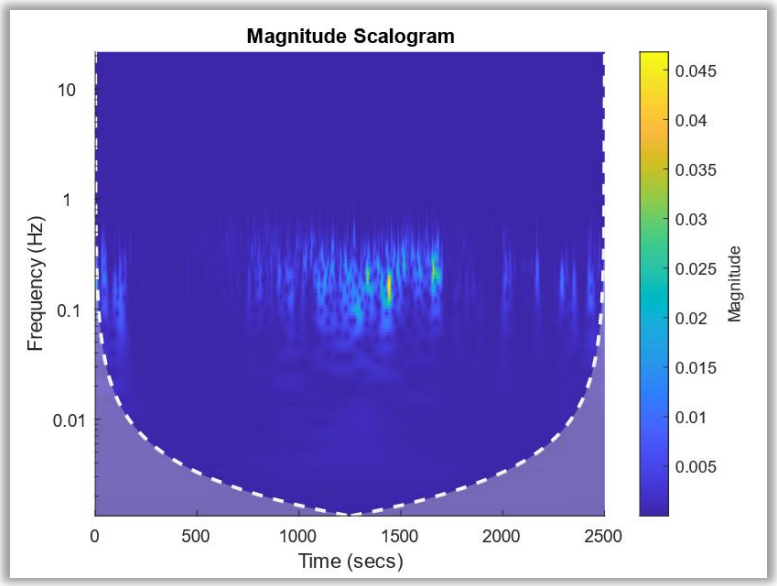

Figure 4.11 Magnitude scalogram obtained by applying EMD to the y-axis angular velocity parameter and then applying CWT to IMF-4

Two of the magnitude scalogram graphs obtained by applying CWT to the selected IMF after the EMD process are given in Figure 4.10 and Figure 4.11.

Consequently, for the first variation of the proposed methods, a total of 105 IMFs belonging to seven different parameters were analyzed by performing wavelet transformation. Following the analyses carried out, three basic inferences were made and the analysis was concluded.

As the second variation of the proposed methods, this time the VMD process was applied to the raw state of the seven parameters to which the EMD process was previously applied. With the inference obtained from the previous analysis, VMD with 5 IMFs was performed for each parameter. Then, CWT process was applied to a total of 35 IMFs obtained for seven parameters. CWT conversion results were analyzed as in the first variation. According to the analysis results, the effectiveness of the three parameters selected for examination was confirmed. Additionally, the most suitable VMD modes for examining turbulence effects were found to be the second and third modes. In other modes, varying frequencies and magnitudes were detected, independent of the turbulence intensity.

Two of the magnitude scalogram graphs obtained by applying CWT to the selected IMF after the VMD process are given in Figure 4.12 and Figure 4.13.

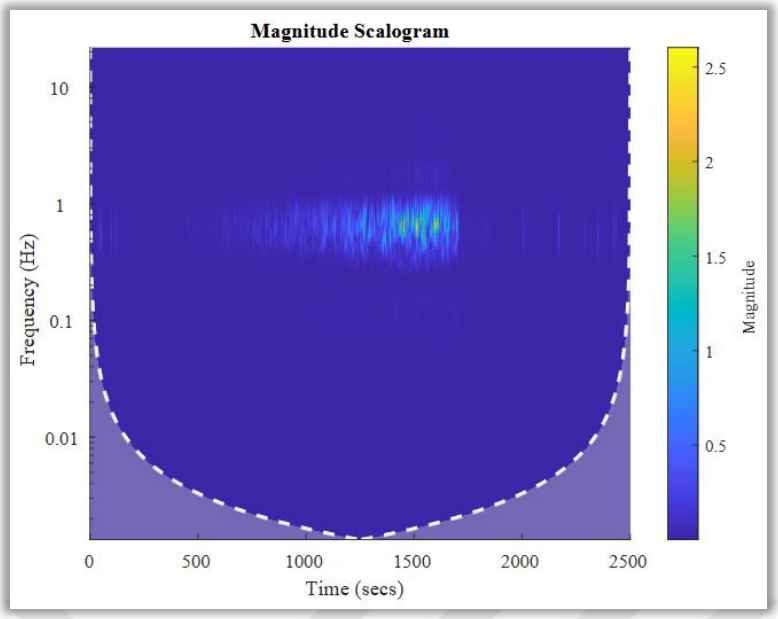

Figure 4.12 Magnitude scalogram obtained by applying VMD to the z-axis lineer acceleration parameter and then applying CWT to IMF-3

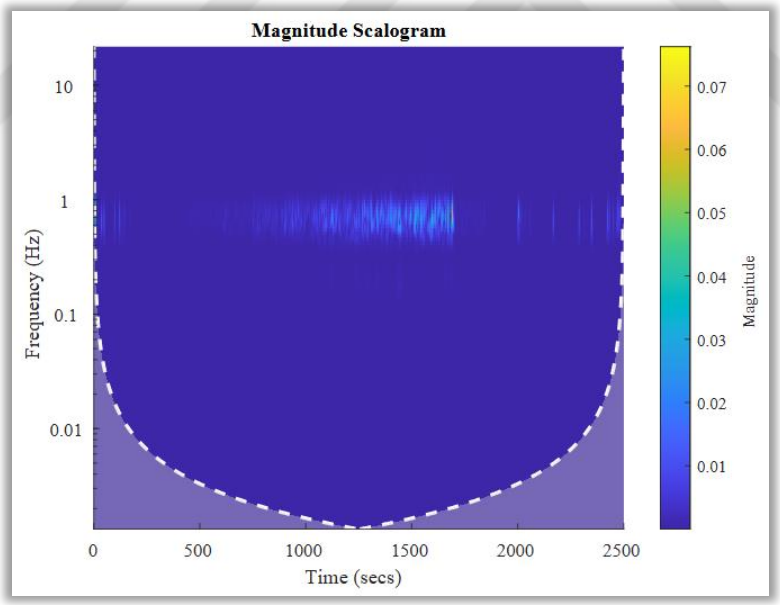

Figure 4.13 Magnitude scalogram obtained by applying VMD to the y-axis angular velocity parameter and then applying CWT to IMF-3

Consequently, for the second variation of the proposed methods, a total of 35 IMFs were analyzed by performing wavelet transformation as the output of the VMD process for seven different parameters. According to the results of the analyses, the

parameters and modes that needed to be examined were determined and the analysis was finalized.

As the next step of the application, the turbulence intensity will be determined. For this purpose, first of all, a MATLAB script was prepared to perform the analysis. There is a main loop that runs in the script. Each element of the simulation time data sequence recorded with flight data corresponds to one rotation of the loop. The data to be processed is fed into the main loop in synchronization with the time sequence. Since the recorded flight data is sampled at 50 Hz, the frequency of the main loop is also 50 Hz. In the main loop, there is a buffer that holds 10 seconds of data. This works out to five hundred samples in total when used with a data set with 50 Hz sampling. At each new cycle, the first data in the buffer is deleted, the data is shifted one row at a time, and the sample in that cycle is added to the last vacant data slot. This 500-element dataset is the new dataset to be processed at each acre. While selecting the number of elements of the buffer, suitability for the processing capacity in embedded systems and the frequency ranges to be examined were taken into consideration. Thanks to the 10-second buffer used here, the minimum frequency value that can be examined is set to 0.1 Hz. Additionally, since the data sampling frequency is 50 Hz, the Nyquist frequency is 25 Hz. This means that the maximum frequency that can be examined with CWT is 25 Hz. The 10 seconds selected for determines the frequency resolution to be obtained in CWT conversion.

The calculation of the minimum observable frequency value is given by Equation (4.6).

$$Frequency\ Resolution = \frac{f_{sampling}}{N_{data}} \tag{4.6}$$

Here, $f_{sampling}$ refers to the recording frequency of flight data. This value as used in the study is 50 Hz. N_{data} refers to the number of elements of the dataset to which CWT will be applied. As used in the study, this value is 500, which is the number of elements of the buffer. In this case, the minimum frequency that can be examined as a result of CWT with the MATLAB script created is 0.1 Hz. According to the general principle of the CWT process, time resolution is increased by increasing the $f_{sampling}$ parameter in the formula given in the Equation (4.6). Thus, shorter-term changes are also evident in CWT results. Changing the N_{data} parameter increases

the time frequency resolution. Thus, changes occurring at lower frequencies become visible in CWT results. These parameters that determine the Time-Frequency resolution are determined according to the type of data to be converted to CWT and the target of the analysis.

Continuing with the explanation of the working principle of the MATLAB script, let it be assumed that the EMD variation will be used as the data processing method. The 500-element data set, which is fed externally to the main loop and saved in the buffer, is first put into the EMD process. After the EMD process, the IMF targeted to be examined is taken (Assume that IMF number 3 will be used for this examination scenario) and converted with the CWT process. The elements corresponding to the determined frequency ranges of the magnitude data obtained after the CWT transformation (These frequency ranges were determined during previous analyses. These frequencies indicate in which frequency range in that IMF the turbulence effects are seen in the resulting scalogram graphs) are marked.

For every 10 seconds of data processed, the sum of the magnitudes corresponding to the marked frequencies over the last 2 seconds is found. Since magnitudes are complex components, their norms are taken before finding their sum. As mentioned in previous sections, turbulence effects create chaotic and unpredictable signals. Here, a cumulative total of 2 seconds is used to ensure that the established system is less affected by instantaneous and irregular changes. Thus, it is aimed to obtain a more stable result in determining the turbulence intensity. The values obtained by summating the last two seconds at each cycle of the main cycle are recorded as the raw turbulence intensity signal.

The MATLAB script, in which the working principle is explained, was run for a total of 12 IMFs determined to be examined in the previous sections of the analysis, and turbulence intensities were obtained. Some of the turbulence intensity graphs obtained are given in Figure 4.14, Figure 4.15 and Figure 4.16. For the ease of comparison, graphs obtained from the results of the process applied to IMF number 3 obtained by applying VMD for all three parameters are given. In all three graphs, it is seen that a directly proportional response is given to the increase in turbulence intensity. On the other hand, the only parameter where the turbulence effect is seen to decrease with the increase in air speed is the angle of attack.

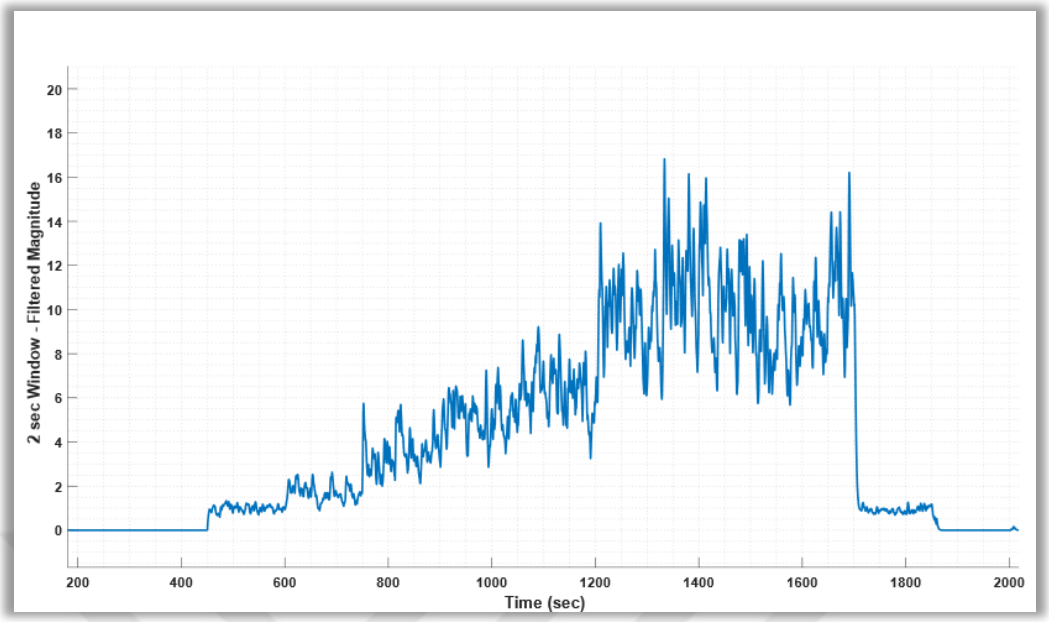

Figure 4.14 Turbulence intensity graph measured by applying VMD to the angle of attack parameter and then applying CWT to IMF-3

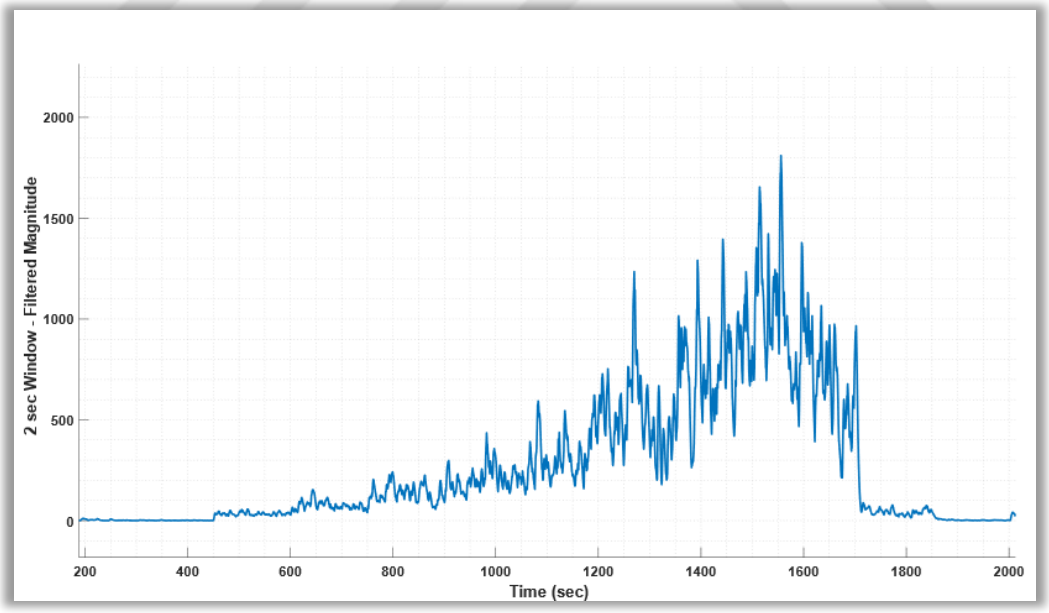

Figure 4.15 Turbulence intensity graph measured by applying VMD to the acceleration in z axes parameter and then applying CWT to IMF-3

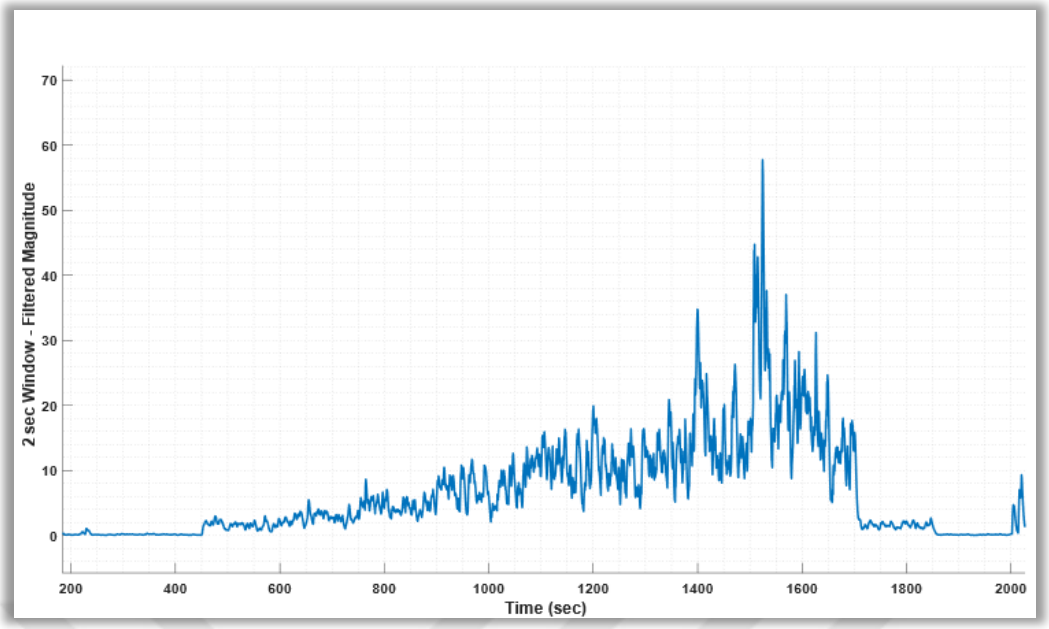

Figure 4.16 Turbulence intensity graph measured by applying VMD to the angular velocity arround x axis parameter and then applying CWT to IMF-3

When a total of twelve graphs of turbulence intensities are examined, it is seen that consistent intensity measurements can be made with many IMFs to the turbulence levels changed during flight. Although the changes in violence are consistent, the magnitudes of violence vary according to the IMF. For this reason, if it is desired to report turbulence levels in the range of 0-7, a calibration must be made that will vary according to the IMF. On the other hand, the results of these 12 IMFs used in the determination should be evaluated and one should be selected to be used in the final system. IMF number 3, obtained as a result of the VMD process of the angle of attack, was selected to be used in the final system. While other IMF results are consistent within themselves, the selected IMF also includes improvements in turbulence effects to a certain extent as the air speed of the aircraft increases. While in some of the other IMFs examined, no change in effect is observed with the increase in airspeed, in others, changes in incomprehensible amounts are observed. As a result of the decision made by evaluating this aspect, the selected IMF will be used as the input of the controller who makes a recommendation regarding the airspeed of the aircraft.

4.2.6 Controller Design

Up to this point in the Application section, collecting flight data, analyzing the collected flight data, and selecting the parameters to be used as a result of the

analysis have been mentioned. In this heading, changes to be made in the aircraft's behavior depending on the turbulence intensity at which the detection process is completed will be discussed.

One of the research questions determined to examine the turbulence problem was whether turbulence effects could be reduced by changes in airspeed. Within the scope of this question, it was decided to design a controller that changes the minimum flight speed of the aircraft depending on the severity of turbulence. The planned controller will work directly by limiting the minimum flight speed of unmanned aerial vehicles that fly with the help of an autopilot system. On the other hand, for aircraft that do not have fully authorized autopilot systems and are operated by a pilot, the controller's outputs will ensure that a minimum flight speed recommendation is made to the pilot in the cockpit.

For the design of the controller, its type must first be determined. One of the two fundemental approaches that can be determined for this is that the controller works based on an online model, and the other is that it works based on measurements taken instantly from the system. The model-based controller structure was not preferred because turbulence effects are unpredictable on the aircraft and running realistic turbulence models in real-time systems requires high processing power. Thus, it is aimed to reduce system complexity and reduce development costs. In this case, the other option will be continued with the measurement-based controller structure. The system diagram, including the controller, is shown in Figure 4.17.

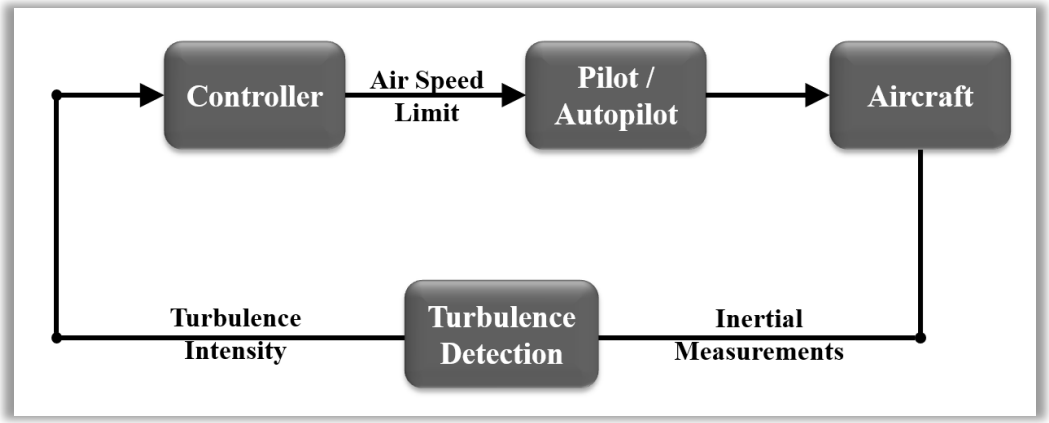

Figure 4.17 The system diagram with controller

A feedback controller will be designed with the selected measurement-based controller structure. At this point, PID-derived controllers come to the fore due to

some factors such as the ease of the development process and the fact that they do not increase system complexity. A PID derived controller has three basic components. The first of these is the proportional term, which allows reacting to instantaneous errors. The second component is the integral component. The integral component contributes to the controller output by collecting all historical errors. Although it is effective in eliminating steady-state errors in the system, it may also cause performance degradation in case of sudden changes since it is a variable with memory. Therefore, its use in this study is not recommended. The third component is the derivative component. The Derivative component calculates the change of the error by comparing the instantaneous error with the error calculated in the previous step. Changing the error improves the performance of the output signal by providing insight into where the system is going. However, it was not preferred to be used in this study due to some reasons such as the error signal being too noisy or having rapid changes. As a final case, it was decided that the designed controller would be a feedback P controller.

In the previous headings, how turbulence intensity is measured with the virtual detection method and the process steps have been mentioned in detail. Since turbulence intensity is obtained from quantities that directly affect the aircraft, it will be considered as a feedback measurement and used at the input of the controller. As mentioned in the previous sections, in flight simulations, the effects of turbulence on the aircraft are directly modeled as linear velocity and angular velocity in the wind frame. Angular velocity affects the attitude angles of the aircraft and, accordingly, the direction of movement. Linear speed causes changes in the air speed of the aircraft. All aerodynamic forces and moments occurring on the aircraft are directly proportional to the square of the air speed. All aerodynamic forces and moments are calculated directly as the dynamic pressure multiplied by other parameters. The formula of dynamic pressure is given by Equation (4.7).

$$q = \frac{1}{2} \cdot \rho \cdot v^2 \tag{4.7}$$

Here, q is the dynamic pressure, ρ is the air density in the environment where the aircraft is located, and v is the true airspeed (TAS).

From a broader perspective, the aim of this study by changing the minimum flight speed of the aircraft is to ensure the balance of force and moment on the aircraft.

Increasing air speed provides the creation of controllable aerodynamic forces and moments that can balance them in response to the unpredictable aerodynamic forces and moments created by turbulence on the aircraft. The mathematical representation of the controller designed for this purpose is given in Equation (4.8).

$$v_{IAS\_min} = v_{stall} + \left(\sqrt{I_T} \cdot K_p\right) \tag{4.8}$$

Here, v_{IAS_min} indicates the minimum IAS value recommended for the aircraft, v_{stall} indicates the IAS value at which the aircraft begins to lose its ability to carry itself, I_T indicates the turbulence intensity and K_p indicates the coefficient of the feedback P controller.

Explanations can be made on the design decisions taken based on the controller's last equation given in Equation (4.8). As seen in the equation, the input of the feedback controller is the square root of the turbulence intensity. As mentioned, turbulence causes changes in the speed of the aircraft. Directly proportional to the square of this speed change, the forces and moments induced on the aircraft provide the system with vibrations measured by IMU sensors. In this case, the turbulence intensity value obtained is actually a quantity that includes the square of the air speed resulting from turbulence. Using turbulence intensity directly to change air speed values will cause forces and moments to be induced on the aircraft in direct proportion to the square of these values. Given these conditions, the change that the controller provides on the forces and moments of the aircraft will become terms containing the fourth power of the airspeed values distorted due to turbulence. As a result, the recommended minimum IAS values will increase exponentially as the turbulence intensity increases. Exponentially increasing minimum IAS values do not meet SEAT's goal of flying at as low a speed as possible, which is one of the initial flight criteria. For this reason, contrary to the common practice in feedback controllers, the square root of the error value, rather than the error value itself, was used as the controller input.

Moreover, there are two variables that need to be determined in order for the controller's equation to take its final form. One of them is the v_{stall} parameter and the other is the K_p parameter. Stall speed is a characteristic of the aircraft used. The stall speed of the modeled aircraft subject to this study is 41 m/s. The K_p value, which is the coefficient of the controller, was selected as 1.703 by trial-and-error

method to provide the best performance during testing and analysis. The first performance criterion evaluated at this point is that the angle of attack does not exceed 7 degrees, which is the stall value. The second performance criterion is the closeness of the aircraft's minimum speed to the stall speed. Efforts have been made to optimize these two performance criteria in the selection of the controller coefficient.

When the stall speed value of the aircraft under study and the coefficient value selected for the controller are substituted into Equation (4.8), Equation (4.9) is obtained.

$$v_{IAS\_min} = 41 + \left(\sqrt{I_T} \cdot 1.703\right) \tag{4.9}$$

Thus, the final ready-to-use version of the controller was obtained.

Using Equation (4.9), the minimum IAS value at which the aircraft can fly safely within the current turbulence effects can be calculated. However, as mentioned before, turbulence effects are chaotic and irregular effects. For this reason, the minimum IAS values obtained are likely to be too variable and noisy. It is difficult for a pilot, who has many different parameters to focus on during flight, to keep the air speed at this value by monitoring a constantly changing and noisy value. For this reason, it is not appropriate to transfer the minimum IAS recommendation to the cockpit in its raw form.

To simplify pilots' workload and to give more applicable IAS recommendations, it was decided to filter the minimum IAS value obtained. The raw value was passed through a first-order low-pass filter and noise factors were removed from the signal. The settling time provided by the low-pass filter used for the current operating frequency is 2 seconds. Additionally, each element of the filtered minimum IAS signal is rounded to its nearest integer value that is greater than or equal to it. This reduces the variability in the signal and makes it easier for the pilot to follow. The final processed minimum IAS value obtained is ready to be transferred to the cockpit to be displayed to the pilot.

4.3 Test and Results

Until this part of the fourth chapter, the problem has been defined, the goals have been determined, the theoretical background has been discussed and the application studies for the solution of the problem have been mentioned. As a result of these studies, the methods, and procedures to be used in solving the problem were determined and the design steps were discussed in detail. In this section, the processes of carrying out a flight test in which the results will be obtained by applying the determined solution methods will be mentioned, and then the proposed methods will be tested with the data obtained from this flight test.

4.3.1 Flight Test

In the previous headings, flight data made with a SEAT modeled in a specified simulation environment were examined. These datas were analyzed and examined offline and were used as training data for the method developed within the scope of the study. In this section, a real-time flight will be carried out with the developed method and the flight data will be presented and analyzed in terms of performance.

The test flight will be carried out in the simulation environment previously described in "4.2.5 Data Collection and Analysis" and using the same model aircraft.

The algorithm that detects turbulence intensity in real time and gives advice to the pilot about the minimum IAS that should be provided during the flight is integrated into the flight simulation. In this context, a subsystem block was created in the simulation environment. Three angular velocity signals and three linear acceleration signals coming from the IMU sensor model were connected to the input ports of the created block. The recommended IAS value was taken into the simulation environment from the single output port in the block, allowing the pilot to easily see this value with the help of a display block.

Within the block, the pitch angle of the aircraft and the direction of the velocity vector were calculated from the acceleration and angular velocity signals received from the input ports. Then, the angle of attack was obtained by taking the difference of these two calculated angles. The obtained angle of attack was transferred to a 500-element buffer that has the capacity to store the last 10 seconds of data, and the data in the buffer was updated at each simulation step.

VMD was applied to the 500-element data set obtained with the help of buffer for each simulation step. The third IMF with 500 elements of the angle of attack signal, which was divided into 5 sub-IMFs with the help of the VMD method, was recorded in a memory variable. Then, CWT was applied to this IMF data. As a result of CWT, a magnitude matrix, a frequency array with as many elements as the rows of the matrix, and a time series with as many elements as the number of columns were obtained. Afterwards, the values of the obtained magnitude matrix corresponding to the frequency values between 1 Hz and 5 Hz were found. A total was obtained by adding up all the elements of these values that fell within the last two seconds. This total obtained is the raw turbulence intensity calculated for that process step of the simulation.

The obtained raw turbulence intensity was passed through a low-pass filter with a settling time of 2 seconds, as explained in the previous sections, and the obtained value was rounded to the nearest and larger integer value. Thus, the minimum IAS value, which was ready to be displayed to the pilot in the cockpit, was transmitted to the simulation environment through the output port of the subsystem block.

The simulation is ready with the integration of the subsystem block, which constitutes the minimum IAS recommendation, into the simulation. A sample test flight was performed in the ready-made simulation. Just before the start of the flight test, data recording was started with a recording frequency of 50 Hz to collect data for analysis and diagnostic purposes. Flight testing was conducted in ISA +0 atmospheric conditions. The altitude and airspeed controllers of the autopilot system were activated for the modeled SEAT aircraft. Within the scope of the test flight, the aircraft with a mass of 4072 kg was taken to the runway. After the take-off run and rotation, the aircraft was allowed to climb to 1000 meters barometric altitude and was manually delivered to the flight zone. Upon reaching the flight zone, aileron surfaces were trimmed so that the aircraft had a roll angle of 3 degrees. Then the altitude and speed controllers were activated. While the barometric altitude of 1000 meters was commanded for the altitude controller, the air speed of 41 m/s, which is the stall speed, was commanded for the air speed controller.

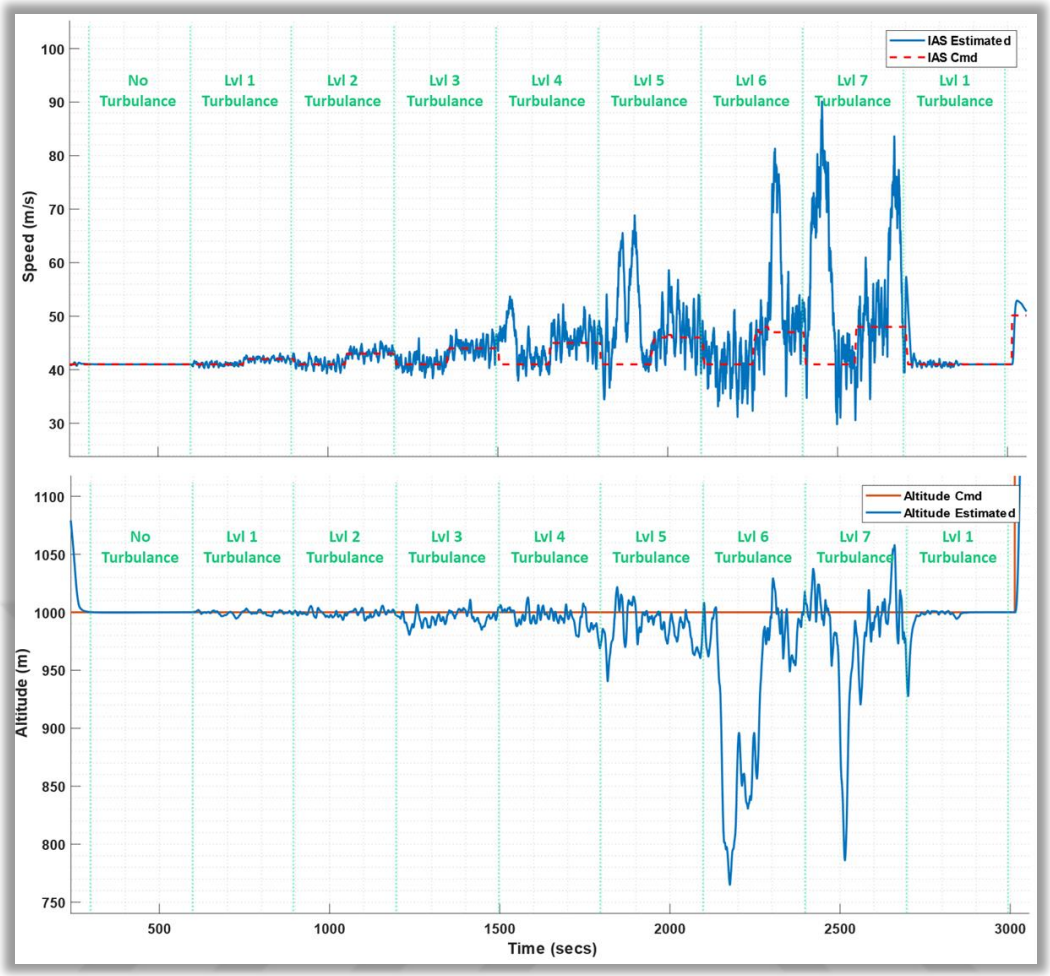

Figure 4.18 IAS (up) and altitude (down) graphs for the test flight (In the graphs, the blue line shows the measured value and the red line shows the command value)

After making the mentioned adjustments, the aircraft started a cruise flight at an altitude of approximately 800 meters above the ground and a barometric altitude of 1000 meters. It was observed that the measured IAS value of the aircraft was 41 m/s and the angle of attack value was 6 degrees. Then the testing procedure was started. Air speed and altitude graphs of the test flight are given in Figure 4.18.

Within the scope of the test procedure, first of all, the aircraft was flown for 300 seconds in windless and turbulence-free atmospheric conditions. During this period, it was observed that the developed algorithm consistently recommended a minimum IAS value of 41 m/s. After the 300th second of the test was reached, the clear air turbulence model was activated and level 1 turbulence was created. The aircraft flew with an IAS command of 41 m/s for 150 seconds in level 1 turbulence. The airspeed controller was then commanded 42 m/s, which is shown as the

minimum IAS recommendation. The aircraft was allowed to fly for another 150 seconds with level 1 tubulence and the recommended IAS command. Thus, the 300-second period in which the effects of level 1 turbulence were tested was completed and the 900th second of the flight was reached. From this point on, the turbulence level was increased for periods of 300 seconds and all turbulence intensities up to level 7 were tested. Finally, the turbulence effect was reduced to level 1, and the flight test was terminated after the aircraft was flown for another 300 seconds. For each level of turbulence intensity, the flight was carried out with a stall speed command of 41 m/s for the first 150 seconds and with the recommended minimum IAS command for the second 150 seconds.

Upon completion of testing procedures with turbulence levels, the aircraft's altitude and speed controller was disabled, it was taken back to the runway and landing was performed. After landing, the mass of the aircraft was measured as 3911 kg. To state it another way, the average mass of the aircraft during the flight can be considered as 4000 kg. Thus, the test flight of the system that detects turbulence intensity and proposes a minimum IAS value accordingly has been completed.

4.3.2 Results

In the previous heading, the integration of the designed system into a flight simulation prepared for a SEAT and the processes of a test flight performed in the simulation were discussed. In this heading, the result graphics obtained from the test flight will be presented. In the first part of the heading, the result graphs presented for the test flight will be evaluated in terms of the system performance observed in the test flight. Then, the IMU graphics obtained from the flight will be analyzed offline and comparative graphics of different methods will be presented, similar to the one in the "4.2 Application" heading.

The analysis begins with an examination of basic measurement data recorded during the flight. Analysis graphs drawn with IAS and altitude data collected during the flight are given in Figure 4.19. In the graphics, blue lines represent measured data and red lines represent command data. Both graphs are divided by vertical lines to show the 300-second periods described in the flight test procedure.

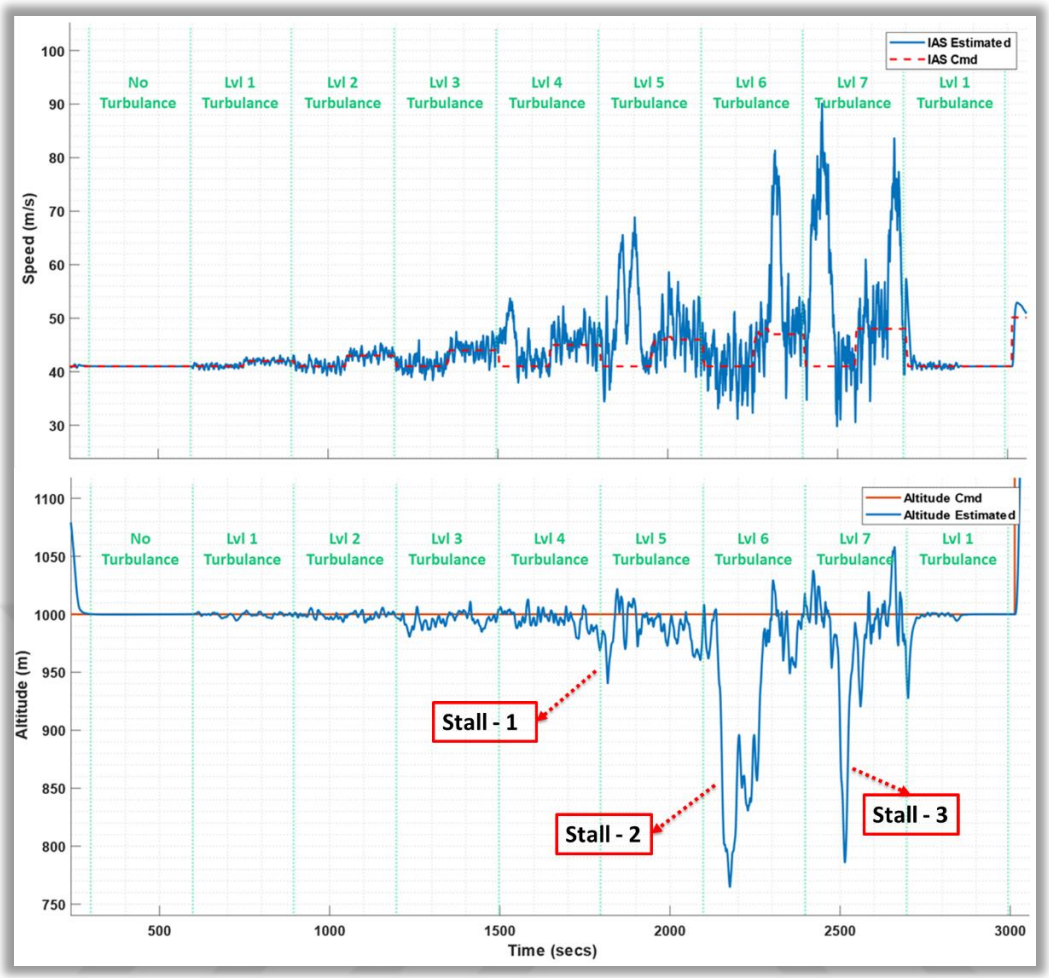

Figure 4.19 IAS (top) and altitude (bottom) analysis graphs for the test flight

When the graphs are examined, it is seen that as the turbulence level increases, the performances of the altitude and air speed controllers are negatively affected. As the intensity of turbulence increased, command tracking decreased as a percentage for both controllers.

It is seen that the air speed controller can follow the air speed commands without any oscillation or steady state error in the non-turbulent period. The first major failure for this controller is seen when the level 4 turbulence intensity is reached. It is observed that in the first part of this period, while the IAS command was 41 m/s, the measured value increased up to 54 m/s with an exceedance of 13 m/s. From a comprehensive view of the IAS graph, it can be seen that the speed command tracking in the second half of each turbulence period is better than in the first half. The only period that is an exception to this situation is the period when level 6 turbulence is applied. In this exceptional period, it was observed that IAS command

tracking was disrupted while trying to maintain the altitude level after the stall effect.

Examination of the altitude graph presented in Figure 4.19 shows that the effects of turbulence levels demonstrate similar patterns to those observed in the IAS graph. While the altitude command can be maintained without oscillation and steady-state error in the first period when there is no turbulence, it is observed that the altitude command tracking deteriorates in the following periods. The aircraft clearly stalled and lost altitude 3 times during the test flight. The first of these events occurred during a level 5 turbulence period and caused the aircraft to lose approximately 60 meters of altitude. Then, it is observed that altitude losses occur during the level 6 and level 7 turbulence periods. In the three stall events observed, the highest altitude loss occurred at approximately 240 meters during the level 6 turbulence period. Conversely, all three altitude loss events occurred in the first half of the turbulence periods when flying with a speed command of 41 m/s. It can be seen from here that the maximum turbulence intensity at which the aircraft can maintain its flight with the determined stall speed in a non-turbulent state is level 4 turbulence.

In order to prove the effectiveness of the proposed system, the effects of the system on flight as well as the events occurring in flight must be examined. The aim of this developed system was to increase flight safety by reducing the amount of the aircraft stalling. For this purpose, in the graphs given in Figure 4.20, the IAS commands suggested by the developed system and the amount of the angle of attack in the stall zone will be examined. In the IAS chart given above in Figure 4.20, the blue line shows the measured IAS, the red line shows the IAS command sent to the air speed controller, and the green line shows the minimum IAS values recommended by the designed system. The graph below shows the angle of attack graph of the aircraft. The blue line in the angle of attack graph shows the calculated angle of attack of the aircraft, and the orange line shows the parts where the angle of attack exceeds 7 degrees, which is the stall limit. As in the previous figure, in the graphs in this figure, 300-second periods with different turbulence levels are indicated by dividing by vertical lines.

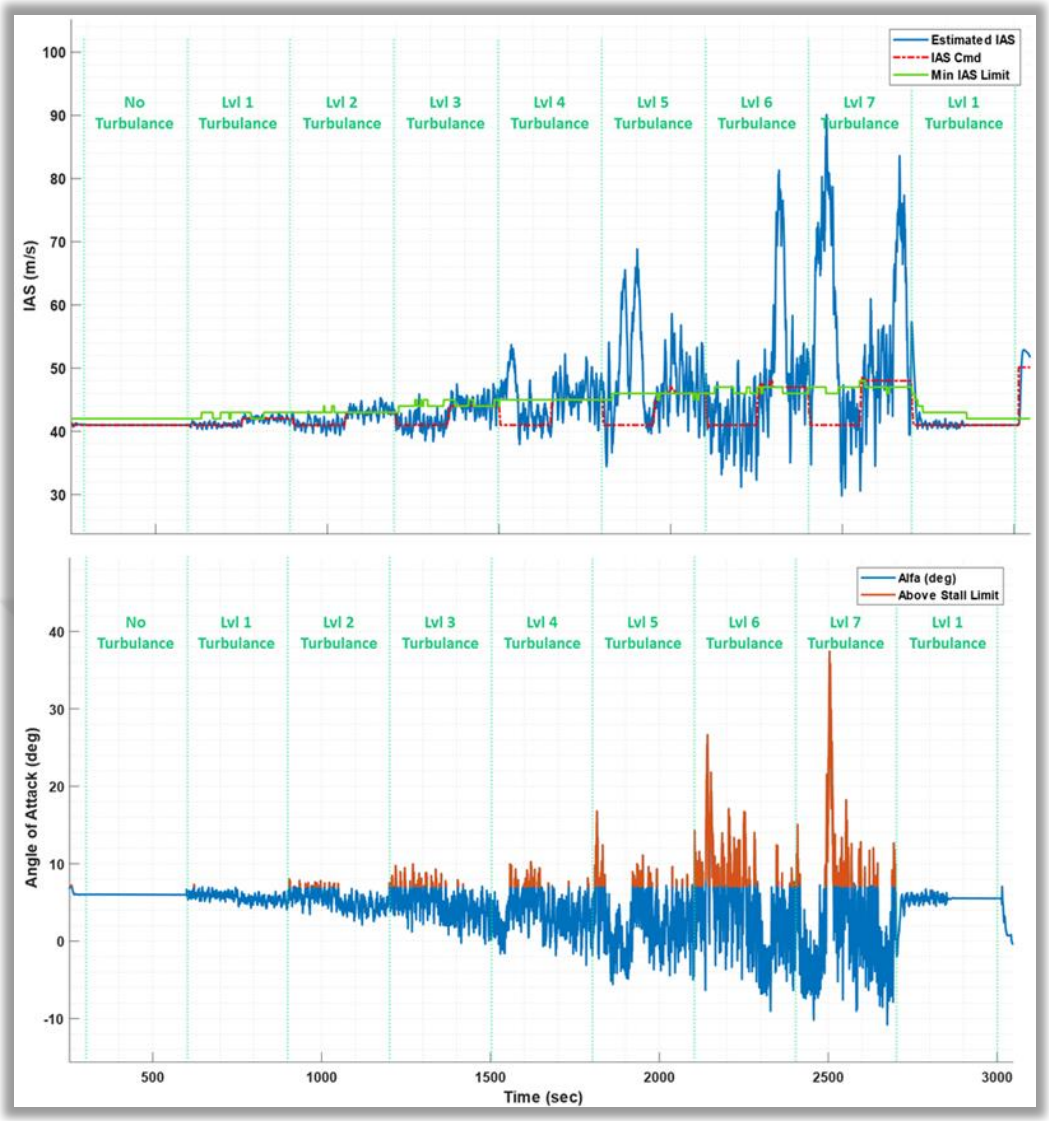

Figure 4.20 IAS (top) and angle of attack (bottom) analysis graphs with the recommended minimum IAS system

Looking at the IAS graph given in Figure 4.20, it can be seen that in the first 150 seconds of each 300-second period, the speed command of 41 m/s is flown, and in the second 150 seconds, the recommended minimum IAS value is used as the speed command.

If the angle of attack graph given in Figure 4.20 is examined, it is seen that the aircraft's angle of attack begins to exceed the stall limit with the level 2 turbulence period. When a general evaluation is made covering all periods, it becomes apparent that the rate of the aircraft exceeding the stall limit decreases significantly in the second half of the periods. Especially in the first five levels of turbulence intensity, by using the recommended IAS value, the angle of attack exceeding the stall limit

was reduced by over 95%. However, this rate is not seen in the same way in level 6 and 7 turbulences. When the reason for this is investigated, it is evident that the aircraft cannot follow the commanded air speed in level 6 and 7 turbulences.

Flight graphics of the system developed up to this point of this title are presented and the results achieved in terms of flight performance are mentioned. As the second part, offline analysis of the data recorded during the flight will be carried out. With this analysis, it is aimed to see how the developed system would perform on the same flight data if it was developed with a different method rather than the recommended method.

In the previous headings of the fourth chapter, three different methods applied to the collected IMU data were presented. The first of these is applying CWT directly to the raw data. The second method is to divide the raw data into sub-modes using the EMD method and apply CWT to the most appropriate IMF. The third method is to divide the raw data into sub-modes using the VMD method and apply CWT to the most appropriate IMF.

The first method whose results will be presented with offline analysis is the method of applying CWT directly to the raw angle of attack data. Scalogram graphs obtained by applying CWT to data collected in different turbulence periods are given in Figure 4.21. Of the four graphs in the figure, the one at the top left was obtained from the data of the 1st level turbulence region, the one at the bottom left was obtained from the data of the 3rd level turbulence region, the one at the top right was obtained from the data of the 5th level turbulence region, and the one at the bottom right was obtained from the data of the 7th level turbulence region. When the graphs are examined, approximately the same behavior is observed with different magnitudes for four different turbulence levels. In the graphs, many different effects can be seen, distributed over a wide band between 0 and 25 Hz frequencies. However, no change effect is observed in the graphs due to the change in air speed at the 150th second of the period.

The second method, the results of which will be presented with offline analysis, is the method of first decomposing the angle of attack data with the EMD method and then applying CWT. In the previous parts of the study, the mode chosen to apply EMD followed by CWT in the use of this method was IMF number 3.

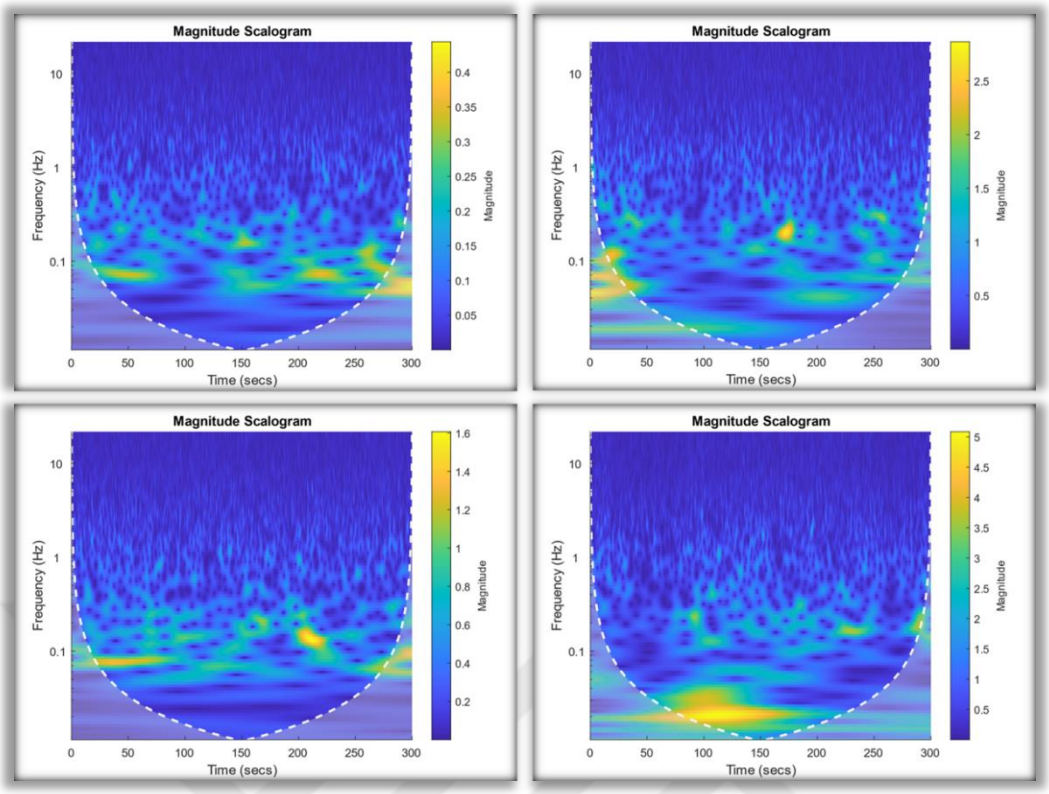

Figure 4.21 Scalogram graphs obtained by applying CWT to angle of attack data collected in different turbulence periods (Top Left: Level 1 Turbulence, Bottom Left: Level 3 Turbulence, Top Right: Level 5 Turbulence, Bottom Right: Level 7 Turbulence)

Scalogram graphics obtained by applying the method are given in Figure 4.22. Of the four graphs in the figure, the one at the top left was obtained from the data of the 1st level turbulence region, the one at the bottom left was obtained from the data of the 3rd level turbulence region, the one at the top right was obtained from the data of the 5th level turbulence region, and the one at the bottom right was obtained from the data of the 7th level turbulence region.

When the scalogram graphs obtained by applying the second method are examined, it is seen that the frequency effects are concentrated in a narrower frequency band compared to the first method. However, although the frequency pattern seen in the graphs for each turbulence level is similar in the first method, it is seen that this situation is different in the second method. Looking at the graph of the 1st level turbulence period on the upper left, it can be seen that there is a dominant effect that is not present in the other graphs at the 150th second of the period. From this perspective, it is observed that the results obtained with this method contain inconsistencies.

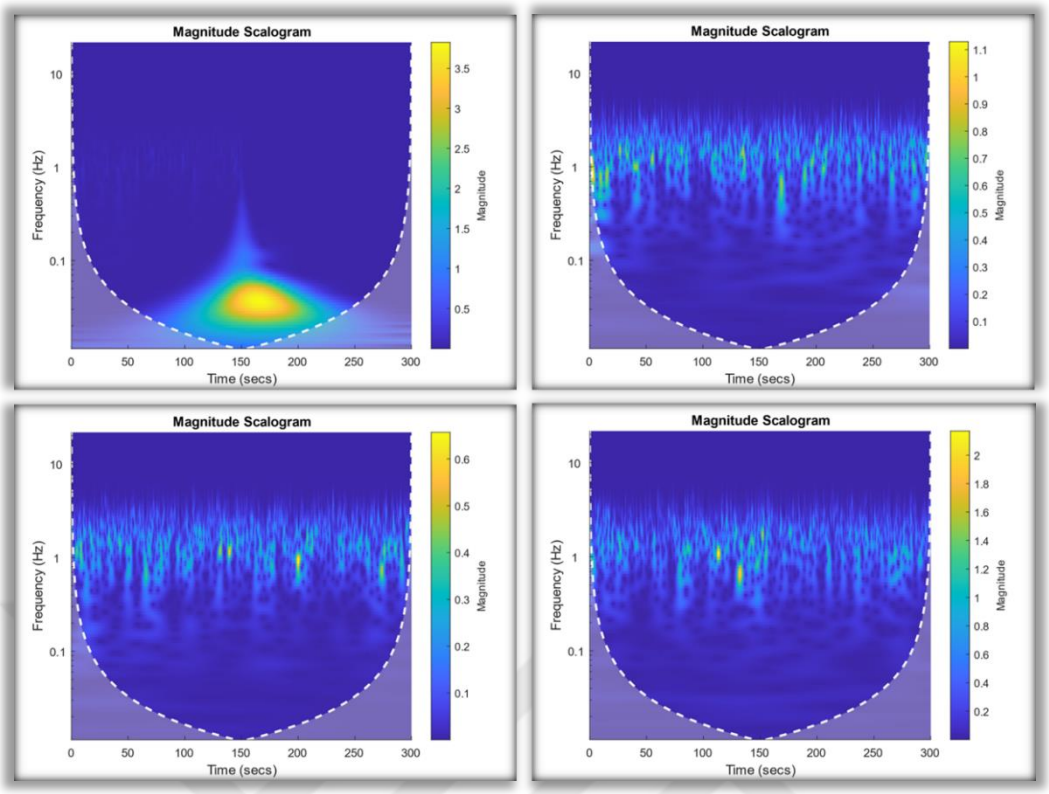

Figure 4.22 Scalogram graphs obtained by first applying EMD and then CWT to angle of attack data collected in different turbulence periods (Top Left: Level 1 Turbulence, Bottom Left: Level 3 Turbulence, Top Right: Level 5 Turbulence, Bottom Right: Level 7 Turbulence)

The third method, the results of which will be presented with offline analysis, is the method of first decomposing the angle of attack data with the VMD method and then applying CWT. In the previous sections of the study, the mode chosen to apply VMD followed by CWT in the use of this method was IMF number 3.

Scalogram graphics obtained by applying the method are given in Figure 4.23. Of the four graphs in the figure, the one at the top left was obtained from the data of the 1st level turbulence region, the one at the bottom left was obtained from the data of the 3rd level turbulence region, the one at the top right was obtained from the data of the 5th level turbulence region, and the one at the bottom right was obtained from the data of the 7th level turbulence region.

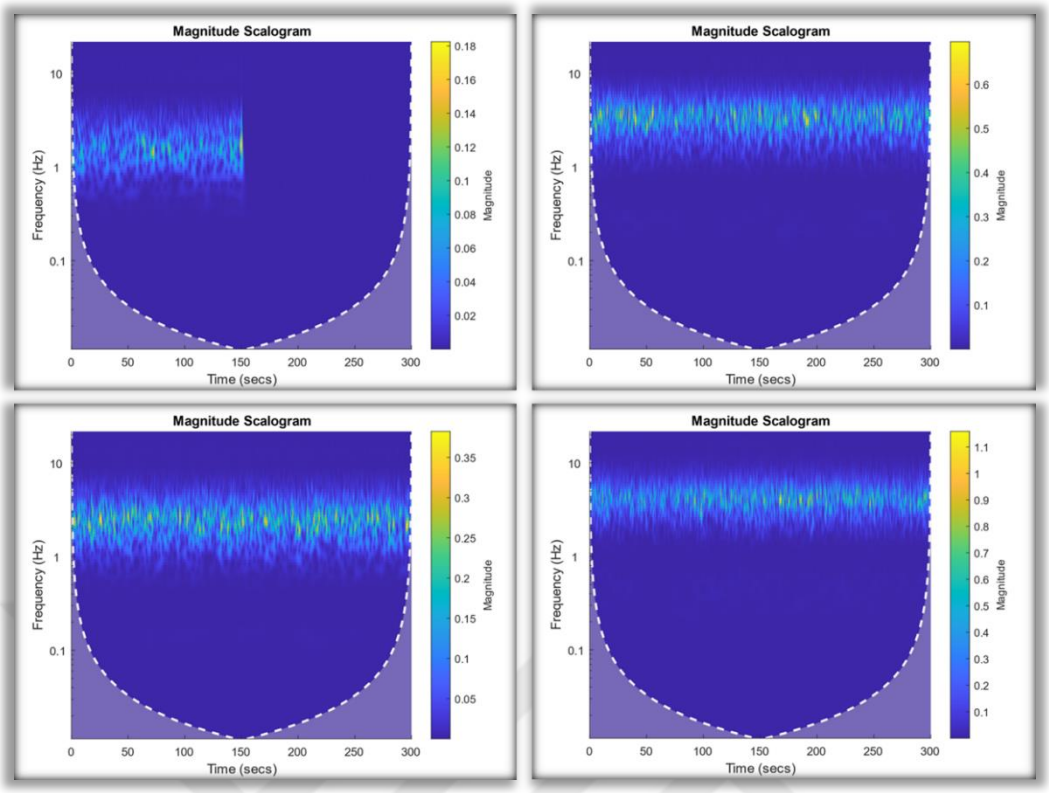

Figure 4.23 Scalogram graphs obtained by first applying VMD and then CWT to angle of attack data collected in different turbulence periods (Top Left: Level 1 Turbulence, Bottom Left: Level 3 Turbulence, Top Right: Level 5 Turbulence, Bottom Right: Level 7 Turbulence)

When the scalogram graphs obtained by applying the third method are examined, it is seen that the frequency effects are concentrated in a narrower frequency band compared to the first two methods. The fact that all regions of the graphs appear dark blue, except those within a certain frequency range, shows that external frequency effects are well separated. Although the magnitudes change in different periods depending on the turbulence levels, it is possible to see the same effects in each graph. As such, the method used provided consistent results for different turbulence levels. In addition, in the 1st level turbulence chart, it is seen that the turbulence effects are compensated and the determined frequency range is cleared by using the recommended minimum IAS value at the 150th second of the period.

The filtered turbulence intensity graph obtained after applying the third method to the angle of attack data recorded in the test flight is given in Figure 4.24. When the graph is examined, it is seen that as the turbulence level increases, the calculated turbulence intensity magnitude also increases. Additionally, for each tubulence level period, it becomes apparent that the turbulence intensity magnitude calculated

in the second half when the IAS commands are changed tends to decrease, albeit slightly.

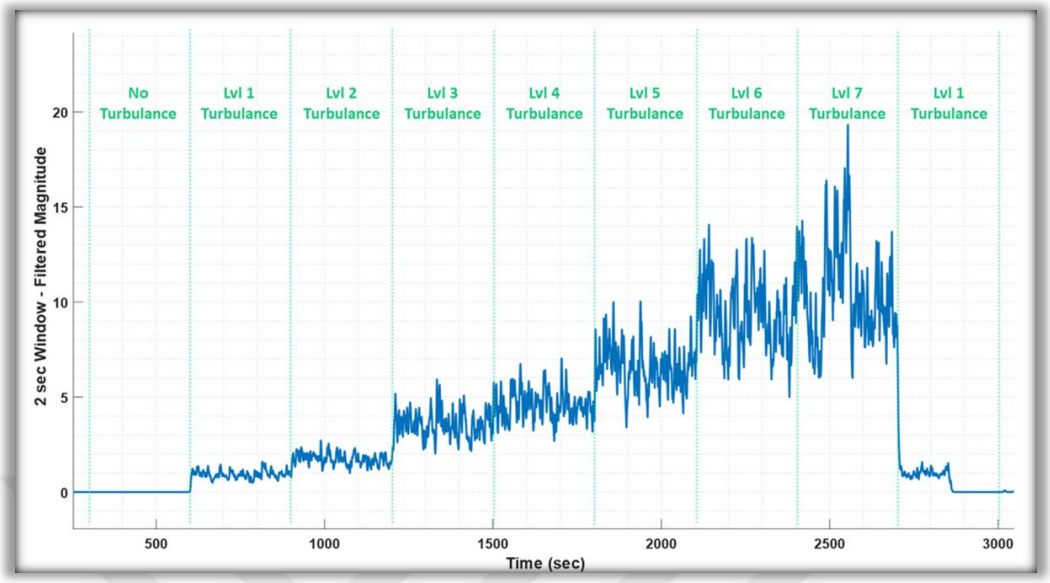

Figure 4.24 Turbulence intensity graph obtained as a result of processing the angle of attack data obtained from the test flight with the recommended method

The result graphs obtained by flight testing are thus presented in terms of flight performance and effectiveness of different methods.

4.4 Conclusion

During Chapter 4, the problem of detecting turbulence intensity in general aviation aircraft and ensuring a safer flight is examined. In the Introduction heading, the problem is defined, the results of the literature research are presented, and research questions are formulated. Then, the infrastructure was created to solve the problem identified in the second heading, Application. In order to better understand the subject, the concept of turbulence was explained and Airtankers selected as a sample study scenario were mentioned. Afterwards, it was mentioned which data would be collected and how to solve the problem, and their theoretical background and reasons were explained. The simulation environment created for the study was introduced, and the tests performed in the simulation environment and the environmental conditions during the tests were mentioned. Three different methods were compared with the data obtained from these tests, and the design steps of the targeted system were discussed by selecting the most appropriate one of these methods. Finally, a test flight was carried out by integrating the designed system

into the flight simulation, and then the resulting data and result graphs showing the effectiveness of the proposed methods were presented.

As a result of this study carried out throughout the fourth chapter, it has been shown that it is possible to measure the severity of turbulence affecting the aircraft using only IMU data. Six different parameters obtained from the IMU sensor and the angle of attack parameter obtained from these parameters were examined within the scope of the study. Based on the investigative findings, it was concluded that the most suitable parameter for turbulence intensity measurement is the angle of attack parameter. Findings reveal that in some of the other measured parameters, the effects depending on the turbulence level show almost no change, and in some of them, it is not appropriate to use the changes seen because they contain inconsistencies.

During the studies on measuring turbulence intensity, the method in the literature (direct application of CWT to the data) was compared experimentally with the proposed methods. As a result of the comparisons, it was concluded that applying CWT directly to an IMU data for turbulence intensity measurement or to the angle of attack data calculated from IMU data cannot perform sufficiently for automatic detection algorithms in measuring turbulence intensity. When EMD+CWT and VMD+CWT methods, which are among the recommended methods, are compared, it is concluded that the VMD method is more suitable for decomposing the signal. The VMD method makes the mode separation in which turbulence effects will be observed in the angle of attack signal more stable than the EMD signal and abstracts the turbulence effects better.

It was seen in the flight test carried out after the system design that the SEAT used could not sustain its flight with the stall IAS value determined under normal conditions due to level 5 turbulence. Conversely, findings indicate that if the speed recommended by the minimum IAS recommendation system integrated into the simulation is used, the aircraft can continue its flight even if stall events occur due to level 6 turbulence. It has been observed that by using the IAS value recommended by the system, the situation of exceeding the stall limit in the angle of attack in the first 5 levels of turbulence is eliminated by up to 95%. According to the operational standards set for SEATs by The National Wildfire Coordinating Group, a US government agency, the flight mission must be canceled if the change

in wind speed exceeds 7.7 m/s (15 knots). Accordingly, a SEAT performing its duty in accordance with standard mission conditions must abort the mission at turbulence levels above level 5. When evaluated from this perspective, the effectiveness of the designed system provides the necessary competence to ensure the safe flight of a SEAT under specified standard mission conditions.

With this study, a new perspective has been added to the literature on the determination of the instantaneous turbulence level affecting an aircraft. Although there are studies in the literature on the determination of turbulence level with the help of signal processing methods of IMU data, there is no other use in the same combination as the methods used in this study. In addition, making an air speed recommendation as a result of the detected turbulence and introducing this system as a product that can operate independently of the aircraft are also contributions to the literature.

In this section, the limiting factors encountered in the solution of this study should also be mentioned. For a signal analysis study, data sampling frequency is always a limiting factor. Frequency effects that could be observed with higher frequency recordings could have enabled the study to reach different dimensions.

Another limiting factor is processing capacity. It is planned to integrate this study into aircraft to run in real time. Therefore, in some design decisions such as the IMF numbers in EMD and VMD decompositions, the size of the buffer used for data storage, and similar design decisions, the choice had to be made based on limited processing capacity. Failure to take processing capacity into account when making these decisions may affect the system performance achieved at the end of the study.

The third limiting factor to be considered is the performance of the altitude and speed controllers of the model aircraft's autopilot. It is seen that controller performances start to decrease significantly, especially when the turbulence level is increased above 5. This situation, which prevented the target air speed values from being achieved, affected the system outputs. Alternatively, despite the fact that there is a possibility of using controllers that will provide better performance, the management of the aircraft under the influence of severe turbulence poses difficulties. Therefore, it should be further discussed how realistic and possible it is to overcome this limitation.

The fourth and last of the most important limiting factors that can be listed within the scope of the study is the turbulence phenomenon itself. Turbulent flow has unpredictable and unstable effects. Therefore, modeling exactly the same as reality is a very difficult problem. The similarity of the Von Karman turbulence model used in the simulation model during the study to a real turbulent flow is a limiting factor for the system. When a system trained according to this model encounters a different structure, it may experience a loss of performance and flight safety may decrease.

Regarding potential future research directions, the first stage will be to test the designed system with aircraft of different models and different turbulence models. Thus, the effectiveness of the proposed method can be verified by examining it under different conditions.

After ensuring the reliability of the proposed method, the second future work will undoubtedly be to test the system on a real aircraft. In this way, processing capacity problems for embedded systems, integration problems for aircraft and problems related to the pilot communication interface will be studied. Another future work that should be evaluated after the system is correctly integrated and its operation is verified is the integration with autopilot systems. The work, which is currently only offered as an auxiliary indicator for the pilot, will be integrated into an autopilot system that can control air speed after passing the necessary reliability stages, and the responsibility on the pilot will be greatly reduced. From the pilot's perspective, this provides extra time and attention that can be devoted to other, more important situations. From an aircraft system perspective, it means increasing the autonomous survivability capabilities of aircraft containing autopilot systems.

Another future study is to measure the advantages that the system brings to the aircraft system in different types of turbulence. Clear air turbulence was studied in this study due to the advantages it provides in terms of modeling and testing. However, when the aircraft in question is a SEAT, there are 3 different types of turbulence that it may be affected by more suddenly and for short periods of time. Systems designed with these types of turbulence should be tested and it should be investigated whether there are parameters that can be optimized in terms of response time or usage.

Consequently, a turbulence intensity detection system, whose effectiveness has been tested and demonstrated, has been developed by using EMD, VMD and CWT methods in appropriate combinations. The output of this developed system is not only a quantity expressing the turbulence level, but also a recommended air speed value for a safer flight, thus reducing the pilot's task load. The existing data and methods obtained and presented have the potential to move forward by providing a basis for future research in this field.

5
CONCLUSION

Throughout this study, efforts have been directed toward developing solutions to address technological and hardware-related disadvantages that compromise the flight safety of general aviation aircraft. The two basic problems identified for this are discussed in Chapter 3 and Chapter 4 and solutions are offered for the problems.

In Chapter 3, an effort was made to detect the moment of ground contact during the descent phase, which is one of the flight phases with the highest accident rate of general aviation aircraft. By evaluating the approaches found in the literature, an approach that would yield the most reliable results at the lowest cost was adopted. Within the scope of the study, a flight simulation and data collected from a Cessna 172SP type general aviation aircraft were used. By using a new approach to process measured signals, accurate detection of the moment the aircraft touches the ground has been achieved through virtual sensing.

In Chapter 4, turbulence, which is one of the situations that most causes fatal and injury accidents in general aviation aircraft, is examined. For the examination, data was collected in flight simulation using a SEAT model used in firefighting activities. By examining the methods in the literature, the virtual detection method was used again in accordance with the initial motivation of the study. A new method has been proposed to determine turbulence intensity by processing IMU data obtained from the aircraft. By using the turbulence intensity measurements of the proposed method, a system that recommends minimum IAS for the safe flight of the aircraft has been developed. The study was confirmed by a test flight and it was seen that the possibility of the aircraft stalling was reduced. The effectiveness of the proposed method compared to other methods has been demonstrated experimentally.

Similar methods were used in studies conducted in two different chapters. With

these studies, a new approach has been introduced to the literature. Signal processing methods such as CWT, EMD and VMD are used in many different applications in many different areas. However, a detection approach made by applying CWT after proper decomposition of a certain signal with EMD or VMD methods is proposed for the first time in these fields.

In forthcoming future studies building on these findings, a suitable goal would be to remove the proposed methods from simulation environments and apply them on real systems. Then, the parameters that need to be optimized when switching between different platforms should be studied. In this way, an aircraft-independent product that can be integrated into all general aviation aircraft can be obtained.

Finally, the targeted due diligence for the general aviation aircraft in question has been successfully carried out and the effectiveness of the proposed methods has been demonstrated experimentally. As a result of these detections made with the virtual detection method, the way is paved for providing higher situational awareness to the pilot and autopilot systems. With the increase in situational awareness, the pilot and autopilot are given the opportunity to intervene more effectively and the aim is to reduce accidents.

REFERENCES

[1] D. Harper, "Etymology of aviation," 1 October 2022. [Online]. Available: https://www.etymonline.com/word/aviation. [Accessed 01 January 2025].

[2] "History of aviation," Wikimedia Foundation, [Online]. Available: https://en.wikipedia.org/wiki/History_of_aviation. [Accessed 1 1 2025].

[3] L. Liu, S. M. Kuo and M. Zhou, "Virtual sensing techniques and their applications," in *2009 International Conference on Networking, Sensing and Control*, Okayama, Japan, 2009.

[4] D. L. Donoho, "De-noising by soft-thresholding," *IEEE Transactions on Information Theory*, vol. 41, no. 3, pp. 613 - 627, May 1995.

[5] D. S. Taubman and M. W. Marcellin, JPEG2000 Image Compression Fundamentals, Standards and Practice, 1 ed., Springer New York, 2002, pp. XXI, 777.

[6] P. S. Addison, "Wavelet transforms and the ECG: a review," *Physiological Measurement*, vol. 26, no. 5, p. 155–199, 8 August 2005.

[7] S. Mallat, "A theory for multiresolution signal decomposition: the wavelet representation," *IEEE Transactions on Pattern Analysis and Machine Intelligence*, vol. 11, no. 7, pp. 674-693, July 1989.

[8] H. Sheikhzadeh and H. R. Abutalebi, "An improved wavelet-based speech enhancement system," in *7th European Conference on Speech Communication and Technology (Eurospeech 2001)*, 2001.

[9] W. J. Staszewski, "Structural Health Monitoring Using Guided Ultrasonic Waves," in *Advances in Smart Technologies in Structural Engineering*, 1 ed., J. Holnicki-Szulc and C. Soares, Eds., Springer, Berlin, Heidelberg, 2004, p. 117–162.

[10] J. B. Ramsey, "Wavelets in Economics and Finance: Past and Future," *Studies in Nonlinear Dynamics & Econometrics*, vol. 6, no. 3, p. 29, January 2002.

[11] Merriam-Webster, "Wavelet," 9 December 2024. [Online]. Available: https://www.merriam-webster.com/dictionary/wavelet. [Accessed 30 December 2024].

[12] A. Grossmann and J. Morlet, "Decomposition of Hardy Functions into Square Integrable Wavelets of Constant Shape," *Society for Industrial & Applied Mathematics (SIAM)*, vol. 15, no. 4, p. 723–736, July 1984.

[13] I. Daubechies, "Orthonormal bases of compactly supported wavelets," *Communications on Pure and Applied Mathematics,* vol. 41, no. 7, p. 909–996, October 1988.

[14] P. S. Addison, The Illustrated Wavelet Transform Handbook, 2 ed., CRC Press, 2017.

[15] R. Polikar, "The Wavelet Tutorial," 06 June 1995. [Online]. Available: https://users.rowan.edu/%7Epolikar/WTtutorial.html. [Accessed 30 December 2024].

[16] Z. Wu and N. E. Huang, "Ensemble empirical mode decomposition: a noise-assisted data analysis method," *Advances in Adaptive Data Analysis*, no. 1, pp. 1-41, January 2009.

[17] Y. Lei, Z. He, Y. Zi and Q. Hu, "Fault diagnosis of rotating machinery based on multiple ANFIS combination with GAs," *Mechanical Systems and Signal Processing,* 2013.

[18] N. E. Huang, Z. Shen, S. R. Long, M. C. Wu, H. H. Shih, Q. Zheng, N. C. Yen, C. C. Tung and H. H. Liu, "The empirical mode decomposition and the Hilbert spectrum for nonlinear and non-stationary time series analysis," *Proceedings of the Royal Society A,* pp. 903-995, 1998.

[19] I. Daubechies, Ten Lectures on Wavelets, SIAM, 1992.

[20] G. Rilling, P. Flandrin and P. Gonçalves, "On empirical mode decomposition and its algorithms," June 2003.

[21] N. E. Huang and Z. Wu, "A review on Hilbert-Huang transform: Method and its applications to geophysical studies," *Reviews of Geophysics,* vol. 46, no. 2, 06 June 2008.

[22] N. Rehman and D. P. Mandic, "Multivariate Empirical Mode Decomposition," *Proceedings of the Royal Society A,* vol. 466, no. 2117, pp. 1291-1302, 8 May 2010.

[23] N. Rehman and D. P. Mandic, "Filter Bank Property of Multivariate Empirical Mode Decomposition," *IEEE Transactions on Signal Processing,* vol. 59, no. 5, pp. 2421-2426, May 2011.

[24] M. E. Torres, M. A. Colominas, G. Schlotthauer and P. Flandrin, "A complete ensemble empirical mode decomposition with adaptive noise," in *IEEE International Conference on Acoustics, Speech and Signal Processing (ICASSP)*, 2011.

[25] X. An and J. Yang, "Denoising of hydropower unit vibration signal based on variational mode decomposition and approximate entropy," *Transactions of the Institute of Measurement and Control,* vol. 38, no. 3, pp. 282-292, July 2015.

[26] D. Zhang and Z. Feng, "Application of variational mode decomposition based demodulation Analysis in gearbox fault diagnosis," in *2016 IEEE International Instrumentation and Measurement Technology Conference Proceedings*, Taipei, Taiwan, 2016.

[27] V. Malhotra and M. K. Sandhu, "Electrocardiogram Signals Denoising Using Improved Variational Mode Decomposition," *Journal of Medical Signals and Sensors,* vol. 11, no. 2, p. 100–107, 24 May 2021.

[28] Y. Diao, J. Lv, Q. Wang, X. Li and J. Xu, "Structural damage identification based on variational mode decomposition–Hilbert transform and CNN," *Journal of Civil Structural Health Monitoring,* vol. 13, no. 6-7, pp. 1-15, June 2023.

[29] S. Lahmiri, "A variational mode decompoisition approach for analysis and forecasting of economic and financial time series," *Expert Systems with Applications,* vol. 55, pp. 268-273, 2016,.

[30] K. Dragomiretskiy and D. Zosso, "Variational Mode Decomposition," *IEEE Transactions on Signal Processing* , vol. 62, no. 3, pp. 531 - 544, February 2014.

[31] X. Xing, M. Wang and W. Zhang, "Adaptive Variational Mode Decomposition for Bearing Fault Detection," *Journal of Signal and Information Processing,* vol. 14, no. 2, pp. 1-8, May 2023.

[32] Y. Ma and S. Cao, "An Improved Robust Threshold for Variational Mode Decomposition Based Denoising in the Frequency-Offset Domain," *Journal of Seismic Exploration,* vol. 28, no. 3, pp. 277-305, June 2019.

[33] Q. Miao, Q. Shu, B. Wu, X. Sun and K. Song, "A Modified Complex Variational Mode Decomposition Method for Analyzing Nonstationary Signals with the Low-Frequency Trend," *Sensors,* vol. 22, no. 5, p. 1801, February 2022.

[34] D. Li, X. Liu, Y. You, D. Zhen, W. Hu, K. Lu and F. Gu, "Rolling Bearing Fault Diagnosis Based on Weighted Variational Mode Decomposition and Cyclic Spectrum Slice Energy," in *6th International Conference on Maintenance Engineering*, Tianjin, 2021.

[35] P. Yuhang, Y. Min and Y. Yan, *Harmonic and Interharmonic Detection in Power Systems Based on Fractal-Optimized Variational Mode Decomposition,* arXiv, 2024.

[36] Y. Guo and Z. Zhang, "Generalized Variational Mode Decomposition: A Multiscale and Fixed-Frequency Decomposition Algorithm," *IEEE Transactions on Instrumentation and Measurement,* vol. 70, pp. 1-13, April 2021.

[37] K. Dragomiretskiy and D. Zosso, "Two-Dimensional Variational Mode Decomposition," in *10th International Energy Minimization Methods in Computer Vision and Pattern Recognition Conference*, Hong Kong, 2015.

[38] European Union Aviation Safeti Agency, "GA Safety Statistics & Main Safety Issues," 3 February 2021. [Online]. Available: https://www.easa.europa.eu/community/content/ga-safety-statistics-main-safety-issues. [Accessed 1 January 2025].

[39] F. L. d. Mello and e. al., "Weight-on-Wheel Detection and Ground-Flight-Mode Switching for UAVs," in *XII Simpiosio Brasileiro de Automacao Inteligente (SBAI)*, 2015.

[40] J. Pytka, P. Budzyński, T. Łyszczyk, J. Józwik, J. Michałowska, A. Tofil, D. Błażejczak and J. Laskowski, "Determining Wheel Forces and Moments on Aircraft Landing Gear with a Dynamometer Sensor," *Sensors,* vol. 20, no. 1, p. 227, 31 December 2019.

[41] T. Masiulionis and J. Stankūnas, "Review of equipment of flight analysis and development of interactive aeronautical chart using Google Earth's software," *Transport,* vol. 33, no. 2, pp. 580-588, 2018.

[42] G. d. RIVALS, "Flight Ops Analysis – Landing Trajectory Computation," in *3rd Conference of the European Operators Flight Data Monitoring (EOFDM)*, Cologne, 2014.

[43] B. KOCA and A. CEYLAN, "Current Status and Recent Developments in Global Positioning Satellite Systems (GNSS)," *Journal of Geomatics,* vol. 3, no. 1, pp. 63-73, 2018.

[44] S. H. Jeong, K. B. Lee, J. H. Ham, J. H. Kim and J. Y. Cho, "Estimation of Maximum Strains and Loads in Aircraft Landing Using Artificial Neural Network," *International Journal of Aeronautical and Space Sciences,* vol. 21, p. 117–132, 2020.

[45] L. Mejias, P. Campoy, K. Usher, J. Roberts and P. Corke, "Two Seconds to Touchdown - Vision-Based Controlled Forced Landing," in *2006 IEEE/RSJ International Conference on Intelligent Robots and Systems*, Beijing, China, 2006.

[46] J. Bakunowicz and P. Rzucidło, "Detection of Aircraft Touchdown Using Longitudinal Acceleration and Continuous Wavelet Transformation," *Sensors*, vol. 20, no. 24, p. 7231, 17 December 2020 .

[47] J. Bakunowicz and P. Rzucidło, "Measurement and analysis of certain flight parameters based on MEMS sensors," *J. Sens. Sens. Syst.*, vol. 6, no. 1, p. 211–222, 12 May 2017.

[48] Laminar Research, [Online]. Available: https://www.x-plane.com/. [Accessed 05 01 2025].

[49] Federal Aviation Administration, "Wake and Weather Turbulence Report," Washington, DC, 2016.

[50] National Interagency Fire Center, "Airtankers," [Online]. Available: https://www.nifc.gov/resources/aircraft/airtankers. [Accessed 05 01 2025].

[51] Wikimedia Foundation, Inc., "Air Tractor AT-802," Wikimedia Foundation, Inc., [Online]. Available: https://en.wikipedia.org/wiki/Air_Tractor_AT-802#. [Accessed 10 01 2025].

PUBLICATIONS FROM THE THESIS

Conference Papers

1. Aircraft Touchdown Detection Using Empirical Mode Decomposition

- *H. Özkaya and U. Sakarya, "Aircraft Touchdown Detection Using Empirical Mode Decomposition," 2024 32nd Signal Processing and Communications Applications Conference (SIU), Mersin, Turkiye, 2024, pp. 1-4, doi: 10.1109/SIU61531.2024.10601088.*